Ore Geology Reviews 141 (2022) 104653

Contents lists available at ScienceDirect

Ore Geology Reviews

journal homepage: www.elsevier.com/locate/oregeorev

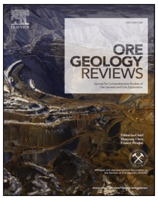

The source, host minerals, and enrichment mechanism of lithium in the Xinmin bauxite deposit, northern Guizhou, China: Constraints from lithium isotopes

Bo Tang [a,b], Yong Fu [a,b,*], Shuang Yan [c], Pei-Wen Chen [a,b], Cheng Cao [d], Chuan Guo [a,b], Pang Wu [a,b], Zhen Long [a,b], Ke-Shu Long [e], Tian-Sun Wang [a,b], Yang Liu [a,b], Ying Yang [a,b]

[a] *College of Resource and Environmental Engineering of Guizhou University, Guiyang 550025, PR China*
[b] *Key Laboratory of Karst Geological Resources and Environment, Guizhou University, Guiyang 550025, PR China*
[c] *Guizhou Central Laboratory of Geology and Mineral Resources, Guiyang 550018, PR China*
[d] *Ministry of Education, Key Laboratory of Surficial Geochemistry, School of G-eological Sciences and Engineering, Nanjing University, Nanjing 210023, PR China*
[e] *Guizhou Geology and Mineral Group, Guiyang 550000, PR China*

ARTICLE INFO

Keywords:
Li isotopes
Li source
Host minerals
Enrichment mechanism
Bauxite

ABSTRACT

Most bauxites in China can be classified as the paleoweathering crust sedimentary type (PCS type) and are normally enriched with lithium (Li). However, the source, host minerals, and enrichment mechanism of Li in bauxites are poorly understood. This study takes the Xinmin bauxite deposit, a typical PCS type in northern Guizhou, China, as a case to trace the Li source and its enrichment using Li isotopes. The Xinmin bauxite deposit is a typical PCS type deposit with high Li contents (average = 756×10^{-6}) and heavy Li isotopic compositions (δ^7Li) (average = 0.83‰). The Hanjiadian Formation's silty shale ($S_{1-2}hj$) and the Huanglong Formation's limestone (C_2h) are the parent rocks of the Xinmin bauxite deposit. The Dazhuyuan Formation (P_1d), as bauxite-bearing rocks of the Xinmin bauxite deposit, was formed via diagenesis from the parent rocks' weathering products. According to the Li isotope fractionation mechanism under chemical weathering, the Dazhuyuan Formation (P_1d) should have a lighter δ^7Li than parent rocks. However, the δ^7Li of the Dazhuyuan Formation (P_1d) is heavier than that of parent rocks, indicating that the Dazhuyuan Formation's original δ^7Li was altered by adding external-source Li characterized by heavy δ^7Li. Considering the sedimentary environment and Li isotopes, this study proposes that the Li carried by surface runoff characterized by heavy δ^7Li is the main source of Li in the Xinmin bauxite deposit. The correlations between clay minerals vs. Li contents and δ^7Li show that illite and kaolinite may be the major host minerals of Li in the Xinmin bauxite deposit. Furthermore, the positive correlations of Li vs. Na_2O and MgO indicate that smectite is another possible Li host mineral. Combined with the formation process of a PCS type bauxite deposit, this study proposes that Li enrichment occurs during the primary bauxitic material formation stage. During this stage, the Li carried by surface runoff converged into the coastal restricted basin where the primary bauxitic materials were deposited. After small-scale transgression, retention water formed in the basin with the rise in the groundwater table. The retained water evaporated under a hot and dry climate, and Li carried by surface runoff accumulated in the basin and was finally adsorbed by clay minerals such as illite, kaolinite, and smectite in the primary bauxitic materials. This mechanism can significantly increase Li contents and δ^7Li in the PCS type bauxite deposit. Additionally, this mechanism implies that the migration process of Li in surface runoff during the formation of primary bauxitic materials determined the present Li contents and δ^7Li of a PCS type bauxite deposit, mainly controlled by the sedimentary environment and hydrologic and climatic conditions at that time.

---

* Corresponding author.
E-mail addresses: btang1@gzu.edu.cn (B. Tang), yfu@gzu.edu.cn (Y. Fu).

https://doi.org/10.1016/j.oregeorev.2021.104653
Received 29 September 2021; Received in revised form 13 December 2021; Accepted 15 December 2021

1. Introduction

Lithium (Li) has two naturally stable isotopes, ^{7}Li (92.41%) and ^{6}Li (7.59%). The large mass difference (~17%) leads to a significant Li isotope fractionation in nature (Pistiner and Henderson, 2003; Rudnick et al., 2004; Huh et al., 2004; Kısakürek et al., 2004, Kısakűrek et al., 2005; Hathorne and James, 2006; Pogge von Strandmann et al., 2006; Vigier et al., 2009; Liu and Rudnick, 2011; Henchiri et al., 2014). Due to their high volatility and being unaffected by a redox reaction or biological process, Li has a few advantages in tracing continental weathering (Rudnick et al., 2004; Tsai et al., 2014; Penniston-Dorland et al., 2017). During continental weathering, ^{6}Li preferentially partitions into secondary minerals, whereas ^{7}Li partitions into the associated water (Kısakürek et al., 2004; Williams and Hervig, 2005; Pogge von Strandmann et al., 2006; Vigier et al., 2008; Teng et al., 2010; Wimpenny et al., 2010, 2015; Hindshaw et al., 2019; Li and Liu, 2020; He et al., 2021; Steinhoefel et al., 2021), resulting in the lighter Li isotopic compositions (δ^{7}Li) of weathering products than parent rocks and surface runoff (Ji et al., 2020). For instance, δ^{7}Li of weathering profiles is lighter than that of fresh diabase, granites, and basalts (Vigier et al., 2008; Pogge Von Strandmann et al., 2006). The δ^{7}Li in altered basalts in Iceland is lower than that in fresh basalts (Pistiner and Henderson, 2003). With the increase in weathering degrees, δ^{7}Li and Li contents decrease gradually from the bottom to the top in the weathering profile of saprolites in South Carolina, United States (Rudnick et al., 2004). However, the δ^{7}Li and Li contents in weathering profiles would change due to the addition of external materials (Huh et al., 2002; Pistiner and Henderson, 2003; Kısakürek et al., 2004; Liu et al., 2013; Ryu et al., 2014; Ji et al., 2020). For instance, the δ^{7}Li in weathering profiles is consistent with or higher than that in fresh basalts developed on Hawaiian basalts due to rain or seawater aerosols (Pistiner and Henderson, 2003; Huh et al., 2004). The abnormal δ^{7}Li at 11 m of a weathering profile developed on the Deccan Trap basalts may be influenced by paleogroundwater (Kısakürek et al., 2004). The relatively higher Li contents and lower δ^{7}Li on the top of the profiles developed on Columbia River basalts than that of fresh basalts indicate the presence of aeolian materials from a weathered ancient continent (Liu et al., 2013). The higher δ^{7}Li in terra rossa relative to the underlying carbonate bedrock in Yunnan, China, could be because of soil pore water diffusion (Ji et al., 2020). Therefore, adding external Li would affect the original δ^{7}Li and Li content of weathering products, providing a way to explore the source and input process of Li in weathering products.

Most bauxites in China are the paleoweathering crust sedimentary type (PCS type), often occurring with abundant Li resources (Zhong et al., 2019), and are natural Li reservoirs. Therefore, it is essential to understand the source, host minerals, and enrichment mechanism of Li in the PCS type bauxite. Not only is it conducive to understanding the Li cycle during the continental weathering process, but also is the premise of exploring and using bauxite associated Li resources. However, a few studies exist on associated Li resources in Chinese bauxite deposits, and the existing understanding is mostly derived from bauxite research. For instance, by studying bauxite material sources, it is considered that the underlying bedrocks are the common material sources of Li-associated resources and bauxites (Jin et al., 2019). Li host minerals are mostly inferred from correlations between Li and other elements combined with Li-ion chemical properties and the mineral compositions of bauxite-bearing rocks (Jin et al., 2019; Wen et al., 2020). Combined with the formation process of bauxites, the Li enrichment mechanism is attributed to weathering accumulation (Jin et al., 2019). Typically, a lack of research on the associated Li resources in Chinese bauxite exists, resulting in scientific problems such as being unable to solve the source, host minerals, and enrichment mechanism of associated Li. The bauxite formation is closely related to continental weathering. The advantage of Li isotopes in tracing continental weathering provides a new means to reveal the enrichment mechanism of associated Li in bauxite. The Northern Guizhou Province Bauxite Belt (NGB), a PCS type bauxite deposit concentration area, is located in the triangle area of Wuchuan, Zheng'an, and Daozhen in the north of Guizhou, China, and enriched with bauxite-associated Li resources (Wang et al., 2013; Jin et al., 2019; Zhong et al., 2019). The Xinmin bauxite is a typical deposit in the NGB, accompanied by abundant associated Li resources with an average content of 756 × 10^{-6}. This study takes the Xinmin bauxite as a case, based on finding the mineral composition, Li content, and Li isotopic composition of bauxite-bearing rocks, combined with previous research results and the fractionation mechanism of Li isotopes during continental weathering to study the source, host minerals, and enrichment mechanism of associated Li. This study should reveal the enrichment mechanism of associated Li in the PCS type bauxite deposit in China and provide useful scientific information for the comprehensive use of associated Li resources.

2. Geological settings

2.1. Regional geology

The NGB is located in the southern margin of the Yangtze Block (Fig. 1a). The oldest rock in the region is the Miaolingian–Furongian Cambrian dolomite of the Loushanguan Formation (Fig. 1b). The Ordovician comprises dolomite, limestone, and claystone. The Lower–Middle Silurian Hanjiadian Formation comprises grayish–green or purplish–reddish silty shale. The Upper Carboniferous Huanglong Formation is micrite limestone. The Lower Permian Dazhuyuan Formation is composed of bauxite-bearing rocks, comprising bauxite ore, bauxitic rock, and aluminous claystone. Bioclastic limestone interbedded with claystone and siliceous rock dominate the strata of Middle–Late Permian, and the bottom unit comprises claystone and carbonaceous claystone interbedded with low-grade coal. The Triassic strata include dolomite, limestone, shale, and sandstone. The Jurassic strata comprise shale and sandstone. During the Late Silurian–Late Carboniferous, a regression caused an epeirogenetic phase and exposed the Hanjiadian Formation to weathering. The limestone of the Upper Carboniferous Huanglong Formation was deposited by short-term transgression during the Late Carboniferous. At the late stage of the Late Carboniferous, regression again caused an epeirogenetic phase and exposed the Hanjiadian and Huanglong Formations to intense weathering from erosion or Karst landform, resulting in the intermittent distribution of the Huanglong Formation. Due to the warm and humid climate, the weathering products experienced strong lateritization to form the primary bauxitic materials. In the following transgression during the Early Permian, the primary bauxitic materials were in situ or transported a short distance and deposited in a semiclosed stable basin (Li et al., 2013), becoming the Dazhuyuan Formation after diagenesis. Folds are common in this region, and the syncline and anticline are arranged alternately in the near NE direction. NNE-trending synclines of the Yanshanian epoch strictly control the bauxitic horizons, and the bauxite deposits (spots) are all hosted in limbs of the synclines (Fig. 1b). The faults in this area were not well developed and mainly developed in a NE direction followed by the NW direction. The influence of faults on bauxitic horizons is limited.

2.2. Deposit geology

The Xinmin bauxite deposit is located in the north of the NGB and the southeast limb of the Datang syncline. The exposed strata include the Lower–Middle Silurian Hanjiadian Formation; the Lower Permian Dazhuyuan Formation; the Middle Permian Liangshan, Qixia, and Maokou Formations; the Upper Permian Wujiaping and Changxing Formations; and the Lower Triassic Yelang Formation (Fig. 1c). The region is typically a monoclinal structure, and the stratum dips 5°–6° toward 275°–350°. The Lower Permian Dazhuyuan Formation is the bauxite-bearing rocks in the region, which unconformably overlie the Lower–Middle Silurian Hanjiadian Formation silty shale or the Late

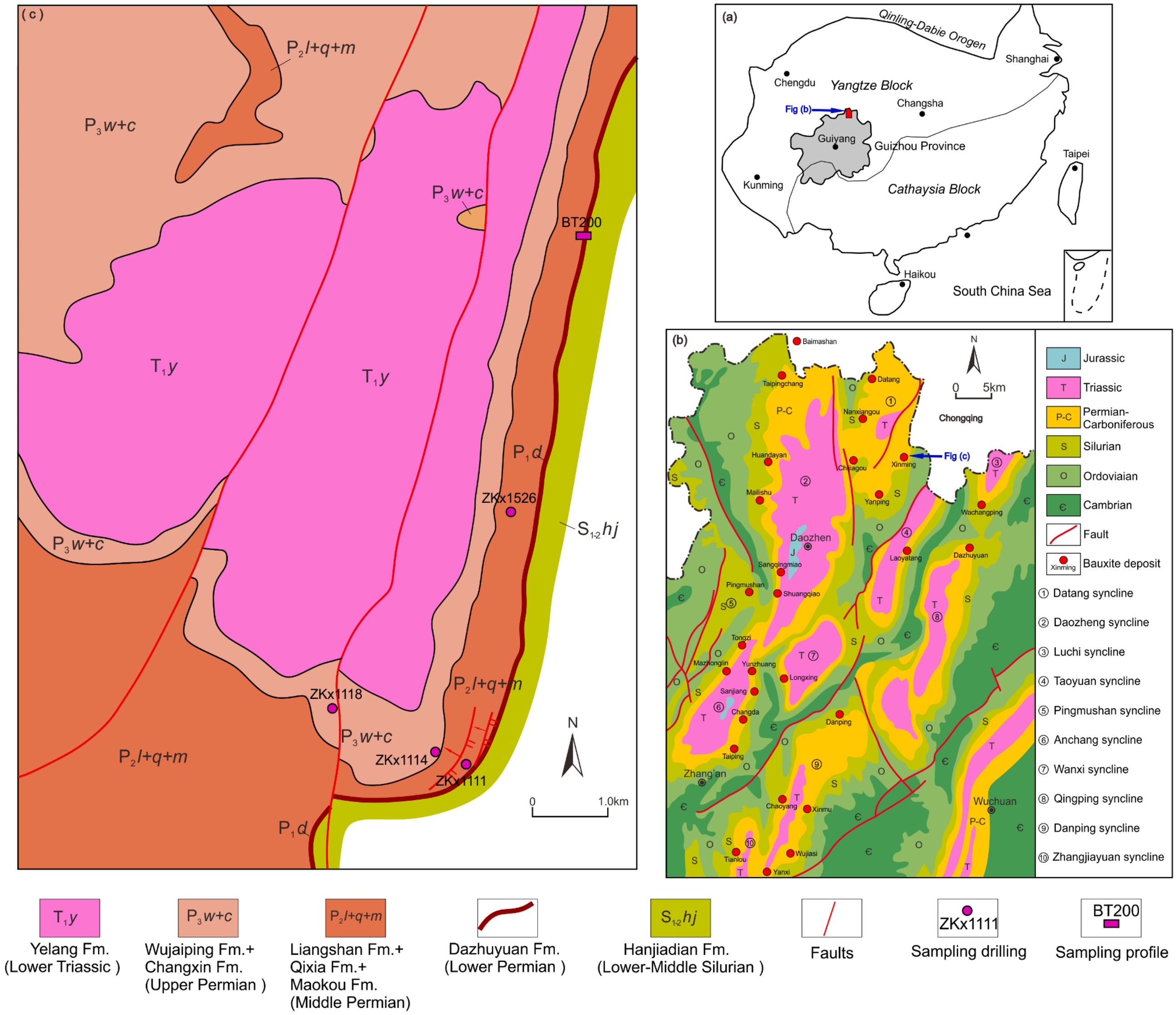

Fig. 1. (a) Inset map of the South China Plate showing the location of the study area. (b) A geologic sketch map illustrating the geological features of the northern Guizhou Province Bauxite Belt (NGB). (c) A geologic sketch map illustrating the geological features of the Xinmin bauxite deposit (Fig. b and Fig. c Modified after Long et al., 2019).

Carboniferous Huanglong Formation limestone in some places. Differences exist in lithological compositions of bauxite-bearing rocks in different areas. The Dazhuyuan Formation, as bauxite-bearing rocks in the NGB, would be divided into three members based on different compositions: (1) the lower member comprising ferruginous claystone, aluminous claystone, and bauxitic rock; (2) the middle member comprising pelitomorphic bauxite ore, clastic bauxitic rock, or pisolitic–oolitic bauxitic rock; (3) and the upper member comprising compact bauxite ore, aluminous claystone, and bauxitic rock. The lithologic association of the sampling boreholes and profile in this study roughly conforms to the above mentioned descriptions (Fig. 2). The ore body is commonly stratiform and stratoid in shape. The NE-trending faults in the region have limited influence on bauxitic horizons but can break the continuity of ore bodies in some places (Fig. 1c).

3. Sampling and analysis methods

The sampling locations are displayed in Figs. 1c and 2. In this study, 56 samples were collected for analysis, among which 48 were collected from 4 boreholes (ZKx1111, ZKx1114, ZKx1118, and ZKx1526) and 8 from the field section (BT200). For whole-rock geochemical analyses, the samples were crushed to 200-mesh using an agate mill. The major element contents of whole-rock samples were evaluated using X-ray fluorescence (XRF) techniques (Shimadzu XRF-1800) by the Beijing Createch Texting Technology Co., Ltd. A sample powder of approximately 0.7 g was weighted and a 7 g composite flux ($Li_2B_4O_7$:$LiBO_2$:LiF = 4.5:1:0.4) was added to the platinum crucible. The sample was heated in a melting machine at 1150 °C until it melted into a liquid. It was analyzed using XRF before cooling and solidifying. The Li contents were analyzed using inductively coupled plasma mass spectrometer (ICP-MS, NexION 300Q) by the National Research Center for Geoanalysis. The ICP-MS measurements were quality controlled using international standard samples OU-6, AMH-1, and GBPG-1 (Potts et al., 2000, 2001; Thompson et al., 1999), and the relative standard deviation was better than 10%. The detailed analytical procedures were described by Franzini et al. (1972) and Qi et al. (2000). The mineralogy compositions of 12 samples were analyzed at the Microstructure Analytical Laboratory using X-ray diffraction (XRD; D/max-rB), operating under 40 kV and 40 mA. The XRD measurements were monitored using the instrument standard Cu Kα target and semiquantitatively calculated using the K-value method. All Li isotope measurements were conducted on a Neptune Plus multi-collector inductively coupled plasma mass

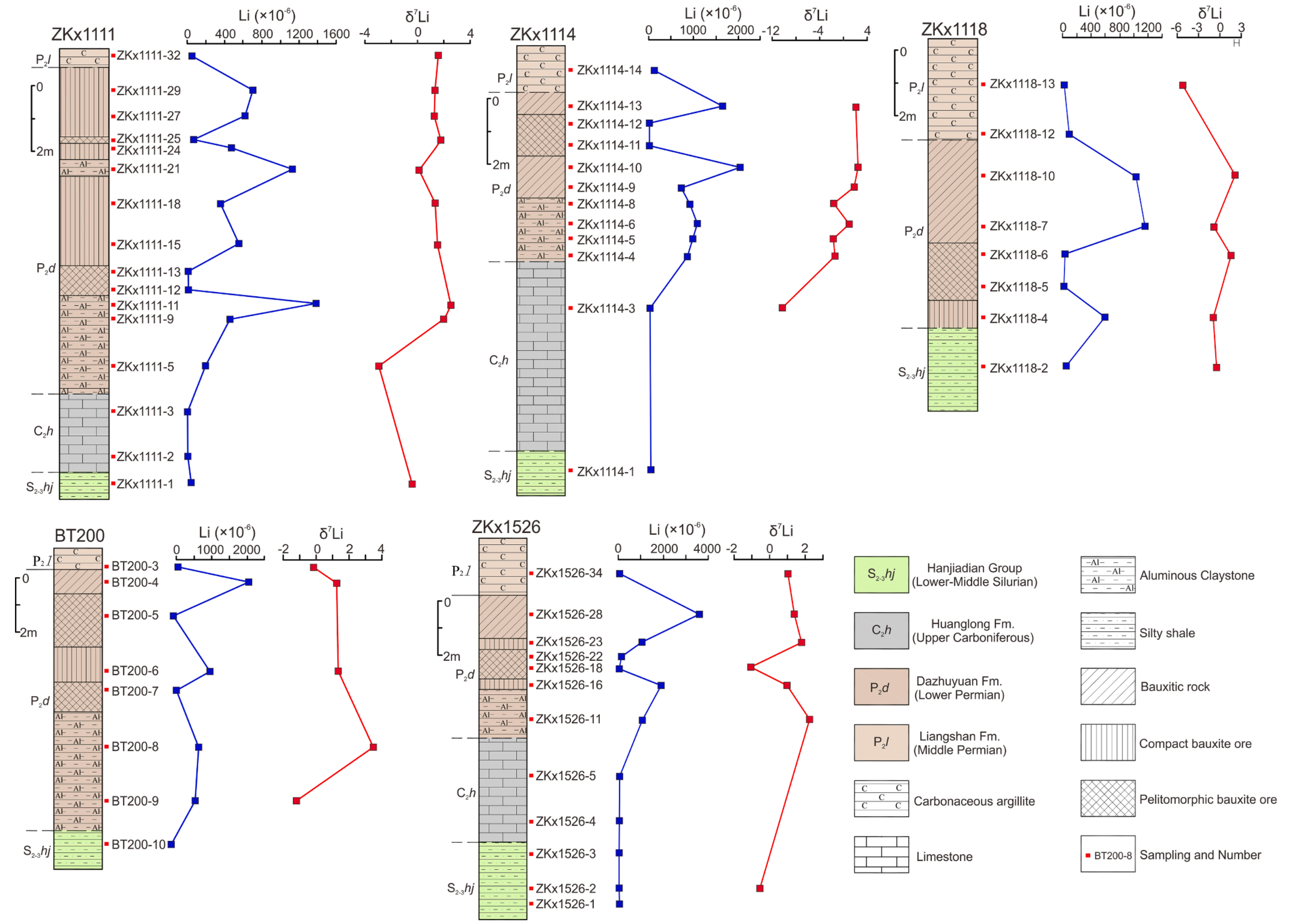

Fig. 2. Lithostratigraphic column for ore-bearing rocks of the Xinmin bauxite deposit, Sampling sites, and the variation relationship between Li contents and δ^7Li.

spectrometer (MC-ICP-MS) equipped with five ion counters and nine Faraday cups at the State Key Laboratory of Continental Dynamics, Northwest University. The measurements were quality controlled using L-SVEC standard sample provided by National Institute of Standards and Technology (NIST). Yan et al. (2020) described the separating and purifying methods for Li isotope analysis of samples and detailed analytical procedures. Furthermore, the bauxitic rock sample with high Li content (ZKx1526-28) was selected to construct polished thin sections for scanning electron microscopy (SEM) (Zeiss sigma 500 field emission) equipped with an energy dispersive spectrometer (EDS) (SEM-EDS) analysis at the National Research Center for Geoanalysis, focusing on observing clay minerals.

4. Results

4.1. Major elements

Major elements are presented in Table 1. Based on the Al_2O_3, SiO_2, and ratio A/S contents, the rock types of the bauxite-bearing rocks can be divided into aluminous claystone ($Al_2O_3 < 40\%$ or $A/S < 1$), bauxitic rock ($Al_2O_3 \geq 40\%$ and $1.8 > A/S \geq 1$), and bauxite ore ($Al_2O_3 \geq 40\%$ and $A/S \geq 1.8$). Bauxite ore can be further divided into compact and pelitomorphic bauxite ores. In bauxite ores, Al_2O_3 contents range from 42.24 to 80.67 wt%, SiO_2 from 0.87 to 25.98 wt%, TiO_2 from 1.20 to 7.85 wt%, TFe_2O_3 from 0.47 to 14.46 wt%, MgO from 0.09 to 2.20 wt%, K_2O from 0.02 to 1.29 wt%, and the loss-in-ignition (LOI) from 13.64 to 16.64 wt%. In bauxitic rock and aluminous claystone, Al_2O_3 contents range from 25.26 to 48.95 wt%, SiO_2 from 25.69 to 44.55 wt%, TiO_2 from 0.73 to 4.57 wt%, TFe_2O_3 from 0.89 to 32.96 wt%, MgO from 0.27 to 4.52 wt%, K_2O from 0.33 to 3.79 wt%, and LOI from 8.06 to 33.76 wt %. The average of Al_2O_3 is the highest in pelitomorphic bauxite ore and gradually decreases in compact bauxite ore, bauxitic rock, and aluminous claystone. The average of SiO_2, MgO, and K_2O related to clay minerals are the highest in aluminous claystone and decrease from bauxitic rock and compact bauxite ore to pelitomorphic bauxite ore. The variation reflects the decrease in clay mineral contents with the increase in bauxite mineralization.

The overlying carbonaceous shale of the Liangshan Formation has the highest SiO_2 contents, from 22.81 to 45.02 wt%, and other elements, including Al_2O_3 (10.54–27.01 wt%), TiO_2 (0.49–1.24 wt%), TFe_2O_3 (3.70–9.01 wt%), MgO (1.38–2.73 wt%), K_2O (2.64–6.56 wt%), and LOI (11.31–25.57 wt%). The average of SiO_2 in the underlying silty shale of the Hanjiadian Formation is more than 60 wt% (61.52–64.31 wt%), indicating a certain amount of quartz in the rock. Other elements, such as Al_2O_3, range from 14.28 to 18.05 wt%, TiO_2 from 0.72 to 0.79 wt%, TFe_2O_3 from 5.07 to 7.34 wt%, MgO from 2.35 to 3.02 wt%, K_2O from 3.39 to 4.45 wt%, and LOI from 4.40 to 6.34 wt%. The underlying Huanglong Formation limestone has the highest CaO contents, from 39.62 to 55.26 wt%. Other elements are low, such as Al_2O_3 (0.82–5.21 wt%), SiO_2 (0.69–17.14 wt%), TFe_2O_3 (0.37–2.43 wt%), MgO (0.34–0.98 wt%), and K_2O (0.0–1.36 wt%), indicating few clay minerals in the Huanglong Formation's limestone.

Table 1
Major (%) elements composition, Li ($\times10^{-6}$) and δ^7Li (‰) of bauxite-bearing rocks from Xinmin bauxite deposit, northern Guizhou, China.

Sample.	Lithology	Al_2O_3	SiO_2	A/S	TiO_2	TFe_2O_3	CaO	MgO	K_2O	Na_2O	MnO	P_2O_5	LOI	Li	δ^7Li
ZKx1111-1	Silty shale	17.57	63.04	0.28	0.74	6.34	0.36	2.91	4.29	0.15	0.04	0.14	4.76	55.28	−0.43
ZKx1111-2	Limestone	2.49	3.99	0.63	0.10	0.94	50.23	0.66	0.59		0.30	0.32	39.17	8.6	
ZKx1111-3	Limestone	1.83	2.16	0.85	0.07	1.52	52.12	0.54	0.22		0.11	0.02	40.55	10.44	
ZKx1111-5	Aluminous claystone	25.26	25.76	0.98	0.73	32.96	0.32	4.52	1.00	0.05	0.05	0.14	8.06	201.01	−2.96
ZKx1111-9	Aluminous claystone	37.81	44.55	0.85	1.94	0.89	0.14	0.33	1.14	1.29	0.00	0.05	12.00	456.43	2.05
ZKx1111-11	Aluminous claystone	38.78	42.49	0.91	1.92	1.31	0.16	0.47	1.91	1.37	0.00	0.03	11.30	1384.03	2.52
ZKx1111-12	Pelitomorphic bauxite ore	75.94	1.35	56.07	6.92	0.51	0.10	0.10	0.02	0.06	0.00	0.05	14.64	4.37	
ZKx1111-13	Pelitomorphic bauxite ore	77.39	1.23	63.12	5.39	0.66	0.10	0.10	0.02	0.04	0.00	0.05	14.85	7.57	
ZKx1111-15	Compact bauxite ore	74.64	7.50	9.95	1.48	0.50	0.09	0.32	0.47	0.10	0.00	0.04	14.88	551.78	1.50
ZKx1111-18	Compact bauxite ore	75.37	6.96	10.83	1.38	0.47	0.11	0.18	0.76	0.12	0.00	0.03	14.34	355.53	1.33
ZKx1111-21	Aluminous claystone	30.01	29.22	1.03	0.76	2.74	0.20	3.10	0.74	0.19	0.00	0.07	33.76	1127.89	0.10
ZKx1111-24	Compact bauxite ore	54.89	25.98	2.11	3.14	0.67	0.13	0.25	0.16	0.17	0.00	0.07	14.57	458.74	1.36
ZKx1111-25	Pelitomorphic bauxite ore	77.54	1.70	45.56	4.04	0.82	0.10	0.13	0.05	0.04	0.00	0.06	15.41	69.68	1.75
ZKx1111-27	Compact bauxite ore	71.08	10.76	6.61	1.43	0.52	0.10	0.26	1.17	0.11	0.00	0.09	14.18	632.10	1.26
ZKx1111-29	Compact bauxite ore	67.14	11.81	5.69	1.38	1.99	0.31	2.20	0.12	0.02	0.00	0.30	15.42	701.18	1.31
ZKx1111-32	Carbonaceous shale	21.63	44.34	0.49	0.94	6.98	5.21	2.73	5.02	0.18	0.03	0.17	11.78	53.22	1.56
ZKx1114-1	Silty shale	18.05	61.52	0.29	0.79	6.89	0.23	3.02	4.45	0.22	0.03	0.11	4.84	62.47	
ZKx1114-3	Limestone	0.82	0.69	1.18	0.04	0.37	55.26	0.34	0.02		0.08	0.00	42.00	21.45	−10.33
ZKx1114-4	Aluminous claystone	32.32	35.05	0.92	1.55	15.71	0.13	2.53	1.92	0.39	0.02	0.16	10.22	858.36	−1.46
ZKx1114-5	Aluminous claystone	35.92	25.69	1.40	2.17	21.18	0.12	3.08	0.48	0.34	0.03	0.10	11.06	987.97	−1.76
ZKx1114-6	Aluminous claystone	34.82	34.94	1.00	1.64	13.11	0.14	2.16	2.41	0.64	0.02	0.20	9.91	1081.68	0.94
ZKx1114-8	Aluminous claystone	34.19	37.39	0.91	4.17	8.75	0.14	0.85	0.33	0.32	0.01	0.05	13.92	929.35	−1.68
ZKx1114-9	Bauxitic rock	41.75	32.25	1.29	2.36	6.02	0.10	0.27	0.72	0.62	0.00	0.03	16.08	727.39	1.77
ZKx1114-10	Bauxitic rock	48.95	28.84	1.70	3.89	2.18	0.13	0.88	1.51	0.66	0.00	0.02	12.04	2016.48	2.41
ZKx1114-11	Pelitomorphic bauxite ore	73.34	1.84	39.79	7.85	1.95	0.37	0.13	0.06	0.06	0.00	0.07	13.99	4.54	
ZKx1114-12	Pelitomorphic bauxite ore	68.18	2.55	26.78	7.70	3.97	0.29	0.12	0.17	0.05	0.01	0.20	16.15	1.68	
ZKx1114-13	Bauxitic rock	40.60	35.55	1.14	3.23	3.46	0.13	1.38	1.29	0.80	0.00	0.04	13.11	1628.47	2.12
ZKx1114-14	Carbonaceous shale	26.67	39.23	0.68	1.09	9.01	1.05	1.69	6.56	0.48	0.02	0.68	13.15	103.59	
Sample.	**Lithology**	**Al_2O_3**	**SiO_2**	**A/S**	**TiO_2**	**TFe_2O_3**	**CaO**	**MgO**	**K_2O**	**Na_2O**	**MnO**	**P_2O_5**	**LOI**	**Li**	**δ^7Li**
ZKx1118-2	Silty shale	16.68	61.93	0.27	0.72	7.11	0.87	2.78	3.69	0.96	0.07	0.11	4.72	52.3	−0.45
ZKx1118-4	Compact bauxite ore	42.24	22.46	1.88	2.27	14.46	0.24	1.28	0.11	0.11	0.01	0.03	16.64	597.28	−0.91
ZKx1118-5	Pelitomorphic bauxite ore	74.68	3.55	21.04	4.92	1.70	0.11	0.18	0.17	0.09	0.00	0.06	14.59	14.74	
ZKx1118-6	Pelitomorphic bauxite ore	75.29	2.87	26.26	4.62	1.71	0.09	0.15	0.17	0.12	0.00	0.06	15.02	39.86	1.59
ZKx1118-7	Bauxitic rock	41.56	40.27	1.03	1.11	1.34	0.09	0.73	0.95	0.82	0.00	0.06	13.09	1153.64	−0.83
ZKx1118-10	Bauxitic rock	45.47	29.38	1.55	4.57	2.76	0.12	2.77	0.49	0.37	0.00	0.04	13.83	1030.27	2.15
ZKx1118-12	Carbonaceous shale	24.88	42.79	0.58	1.12	7.35	0.46	2.43	5.44	0.50	0.02	0.12	13.28	88.36	
ZKx1118-13	Carbonaceous shale	10.54	22.81	0.46	0.49	3.70	30.75	1.38	2.64	0.08	0.18	0.05	25.57	27.85	−5.23
BT200-3	Carbonaceous shale	27.01	44.28	0.61	1.23	5.19	0.38	1.78	6.05	0.20	0.01	0.11	12.77	65.91	−0.15
BT200-4	Bauxitic rock	48.47	32.25	1.50	1.80	1.26	0.28	0.97	1.78	0.76	0.00	0.02	12.07	1996.47	1.26
BT200-5	Pelitomorphic bauxite ore	80.67	0.87	92.89	2.60	0.57	0.17	0.09	0.02		0.00	0.49	14.53	3.55	
BT200-6	Compact bauxite ore	63.81	16.08	3.97	1.20	1.88	0.28	1.25	1.29	0.20	0.00	0.05	13.64	937.76	1.35
BT200-7	Pelitomorphic bauxite ore	78.97	1.05	74.87	4.90	1.01	0.08	0.10	0.03	0.04	0.00	0.06	14.22	5.34	
BT200-8	Aluminous claystone	35.09	26.19	1.34	2.99	19.83	0.26	0.34	1.69	0.24	0.00	0.07	12.60	526.83	3.48
BT200-9	Aluminous claystone	33.31	35.44	0.94	1.25	10.19	0.40	1.33	3.79	0.72	0.00	1.04	11.21	586.97	−1.19
BT200-10	Silty shale	17.14	62.08	0.28	0.73	7.34	0.44	2.63	4.06	0.56	0.04	0.14	4.40	38.5	
ZKx1526-1	Silty shale	17.73	62.33	0.28	0.75	6.29	0.36	2.90	4.42	0.23	0.04	0.13	4.86	44.61	
ZKx1526-2	Silty shale	14.28	64.31	0.22	0.73	5.07	3.21	2.35	3.39	0.33	0.06	0.15	6.34	37.99	−0.54
ZKx1526-3	Limestone	5.21	17.14	0.30	0.22	2.43	39.62	0.93	1.36		0.21	1.13	31.09	14.95	
ZKx1526-4	Limestone	1.49	13.37	0.11	0.06	1.02	45.06	0.98	0.30		0.32	0.18	36.28	6.8	
ZKx1526-5	Limestone	3.99	5.57	0.72	0.11	1.26	48.61	0.55	0.99		0.05	0.04	38.48	9.7	
	Aluminous claystone	36.20	39.62	0.91	1.60	5.35	0.20	0.87	1.50	1.47	0.00	0.13	12.95	1090.17	2.26

(*continued on next page*)

Table 1 (*continued*)

Sample.	Lithology	Al_2O_3	SiO_2	A/S	TiO_2	TFe_2O_3	CaO	MgO	K_2O	Na_2O	MnO	P_2O_5	LOI	Li	δ^7Li
ZKx1526-11															
ZKx1526-16	Compact bauxite ore	58.69	20.16	2.91	1.99	1.71	0.23	1.14	1.24	0.38	0.00	0.07	14.43	1994.23	0.99
ZKx1526-18	Pelitomorphic bauxite ore	78.05	3.79	20.60	2.82	0.54	0.11	0.10	0.48	0.09	0.00	0.05	14.76	25.66	−1.05
ZKx1526-22	Pelitomorphic bauxite ore	79.86	0.91	87.53	3.61	0.63	0.12	0.09	0.02	0.05	0.00	0.05	15.48	2.75	
ZKx1526-23	Compact bauxite ore	62.15	14.44	4.30	2.10	3.08	0.25	0.64	1.14	0.33	0.00	0.06	15.86	1006.00	1.81
ZKx1526-28	Bauxitic rock	44.15	35.24	1.25	1.06	2.01	0.17	1.81	1.35	0.85	0.00	0.04	13.15	3521.36	1.40
ZKx1526-34	Carbonaceous shale	26.81	41.60	0.64	1.19	7.27	0.37	2.30	6.32	0.38	0.02	0.12	12.66	70.01	1.04

4.2. *Mineralogy*

The mineralogical compositions are tabulated in Table 2 and are displayed in Fig. 3. Pelitomorphic bauxite ores are mostly diaspore, accounting for more than 90%, and the remaining are heavy minerals, such as anatase and rutile. In compact bauxite ores, Al minerals account for more than 80%, dominated by boehmite and a minor diaspore amount. Furthermore, illite and kaolinite dominate clay minerals and there are a few heavy minerals. The most important feature of bauxitic rocks is the complex composition of Al and clay minerals. Al minerals include diaspore, boehmite, and gibbsite, and clay minerals include illite, chlorite, and kaolinite. Aluminous claystone mainly comprises clay minerals, diaspore, heavy minerals, and some rare earth element independent minerals, and clay minerals are mainly chlorite and kaolinite. The mineral composition of the Hanjiadian Formation silty shale comprised quartz, illite, and chlorite with few calcite and feldspar minerals.

Because the clay minerals in bauxite are fine and often exhibit heteromorphic structures, it is challenging to identify them only based on morphological characteristics. However, based on the results of the XRD analysis of sample mineral composition and the difference in chemical compositions of different clay minerals, SEM-EDS analysis can be used to identify clay minerals more accurately. For example, illite is different from other clay minerals due to its higher K; Al:Si in kaolinite is approximately 1:1 without K, and chlorite is rich in Fe or Mg. Although the EDS cannot effectively analyze Li in Li-chlorite, if Li-chlorite would be present in the sample, it could be identified by its special Al:Si ratio (5:3) (Ling et al., 2021).

4.3. *Li and Li isotopic compositions*

Li contents and δ^7Li are tabulated in Tables 1 and 3 and are illustrated in Figs. 2 and 4. The change in δ^7Li has no obvious pattern, but lithology controls the change in Li content, with low values often corresponding to pelitomorphic bauxite ore (Fig. 2). The Li contents of bauxite-bearing rocks range from 1.68×10^{-6} to 3521×10^{-6}, with an average of 756×10^{-6}. Bauxitic rocks show an average of the highest and widest variations in Li concentrations. The δ^7Li of bauxite-bearing rocks ranges from – 2.96‰ to 3.48‰, averaging at 0.83‰, with the highest in bauxitic rock and the lowest in aluminous claystone with the widest variation range. However, no obvious correlation between Li contents and δ^7Li is observed (Fig. 4). Overall, the average δ^7Li of the Xinmin bauxite deposit is close to that of the upper continental crust (0.6‰) (Tomascak, 2004; Misra and Froelich, 2012; Sauzéat et al., 2015) and loess (0.6‰) (Tsai et al., 2014; Sauzéat et al., 2015), but exhibit more consistent δ^7Li compositions (Fig. 5). The average Li content of the overlying Liangshan Formation is 64.89×10^{-6}, ranging from 27.85×10^{-6} to 103.59×10^{-6}, and the δ^7Li average is – 0.69‰, with a wider variation range (−5.23‰–1.56‰). The average Li content of the underlying Huanglong Formation is 12×10^{-6}, ranging from 6.8×10^{-6} to 21.5×10^{-6}. The δ^7Li of the Huanglong Formation from only one sample has extremely low δ^7Li (−10.33‰), exceeding the δ^7Li range in marine sediments and biogenic carbonates (Fig. 5). The reason could be that the whole-rock analysis is adopted for Li isotope analysis, and the obtained δ^7Li is the δ^7Li of clay minerals in the sample. The average Li content of the underlying Hanjiadian Formation is 48.53×10^{-6}, ranging from 37.99×10^{-6} to 62.47×10^{-6}. Li isotope compositions are relatively uniform, from – 0.54‰ to – 0.43‰, and average at – 0.47‰.

5. Discussions

5.1. *Implication of Li sources from δ^7Li*

Some studies have proposed that Li enrichment in PCS type bauxite deposits resulted from accumulating Li-containing clay minerals and significant loss of major elements during the weathering of parent rocks (Jin et al., 2019; Wen et al., 2020; Ling et al., 2018). The Hanjiadian Formation's silty shale and Huanglong Formation's limestone are parent rocks of the Xinmin bauxite deposit and the Xinmin bauxite deposit formed by accumulating primary bauxitic materials formed by the weathering of parent rocks and accompanied by forming many clay minerals (Gu et al., 2013; Jin et al., 2019). If the accumulation of Li-containing clay minerals during weathering leads to Li enrichment, the Dazhuyuan Formation, as bauxite-bearing rocks, should have a lighter δ^7Li than the Hanjiadian and Huanglong Formations. However, the Dazhuyuan Formation displays heavier δ^7Li (average 0.83‰) than parent rocks. Therefore, Li in the Xinmin bauxite deposit should originate from other sources besides the Li-containing clay minerals formed by the weathering of parent rocks. This part of Li is characterized by heavy δ^7Li and enriches Li in the Xinmin bauxite deposit.

During continental weathering, ^{6}Li is preferentially retained in secondary minerals, whereas ^{7}Li enters the associated water (Lui-Heung and Edmond, 1988; Tomascak et al., 2003; Tomascak, 2004; Witherow et al., 2010; Godfrey et al., 2013). Therefore, the δ^7Li of weathering products should be lighter than that of parent rocks (Pistiner and Henderson, 2003; Kısakürek et al., 2004; Liu et al., 2013; Ji et al., 2020). However, since the weathering products are often in an open system, their original δ^7Li could change due to adding external materials (Huh et al, 2002; Pistiner and Henderson, 2003; Kısakürek et al., 2004; Liu et al, 2013; Ryu et al, 2014; Ji et al., 2020), for example, the impact of Li carried by rainwater or seawater aerosols on δ^7Li in the Hawaiian basalt profile (Huh et al., 2004) and the influence of Li carried by surface runoff on the Li contents and δ^7Li of loess in China (He et al., 2021). Therefore, surface runoff with heavy δ^7Li can significantly affect the δ^7Li of weathering products. The Xinmin bauxite deposit formed in the coastal restricted basin (Li et al., 2013). The addition of surface runoff or seawater aerosol might affect the Li contents and δ^7Li in the primary bauxitic materials. Given the Li enrichment and heavier δ^7Li in the Xinmin bauxite deposit than parent rocks, the surface runoff that can carry a large amount of Li with heavy δ^7Li characteristics could be the

Table 2
Abundance (wt.%) of minerals in selected samples from X-ray Diffraction.

Sample	Lithology	Quartz	Plagioclase	Microcline	Calcite	Illite	Chlorite	Diaspore	Anatase	Rutile	Pyrite	Boehmite	Kaolinite	Gibbsite	Florencite
ZKx1526-2	Silty shale	47	4	4	8	21	16								
ZKx1526-22	Pelitomorphic bauxite ore	1						95	2	2					
ZKx1526-28	Bauxitic rock					16	23	24				10	12	15	
ZKx1118-5	Pelitomorphic bauxite ore	1						93	3	2	1				
BT200-4	Bauxitic rock					12	8	9				50	11	10	
BT200-6	Compact bauxite ore					6		12	2	1	2	73	4		
BT200-7	Pelitomorphic bauxite ore							95	3	2					
BT200-9	Aluminous claystone						34	21	11	9			15		10
ZKx1114-5	Aluminous claystone						35	39					26		
ZKx1114-10	Bauxitic rock					18	11	56					15		
ZKx1114-13	Bauxitic rock					18	19	20			8	22	13		
ZKx1111-5	Aluminous claystone						100								

major source of Li in the Xinmin bauxite deposit. However, whether the Li carried by surface runoff could enrich in bauxite was subject to the sedimentary environment and hydrologic and climatic conditions at that time (Section 5.3).

Hence, there were at least two sources of Li in the Xinmin bauxite deposit, namely, parent rocks and surface runoff; however, the surface runoff should be the main source. The Li carried by the surface runoff came from all weathered strata in the study area, including the underlying bedrock of bauxite-bearing rocks. Therefore, the Li source beds in the Xinmin bauxite deposit are not limited to the underlying bedrock.

5.2. δ^7Li indication to the host Li minerals

Studies have shown that Li in bauxite is mostly adsorbed by clay minerals (Karayigit et al., 2006; Wang et al. 2013; Ling et al., 2018; Ling et al., 2020; Ling et al., 2021; Long et al., 2021). The clay minerals of the Xinmin bauxite deposit are mainly illite, kaolinite, and chlorite (Table 2, Fig. 3 and Fig. 6). Illite exists widely in the underlying Hanjiadian Formation silty shale (Table 2); therefore, illite in the Xinmin bauxite deposit might be mostly inherited from the Hanjiadian Formation (Cui et al., 2013). Illite is leaf shaped and closely coexists with kaolinite and chlorite (Fig. 6a–6d). Similar to smectite, illite has a 2:1 layered structure, with strong adsorption and cation exchange capacity. Li content is usually high in samples containing illite, such as ZKx1526-28, ZKx1114-10, and BT200-4 (Table 1). The positive correlation between illite and Li contents (Fig. 7a) indicates that illite is the Li host mineral in the Xinmin bauxite deposit. The positive correlation between illite and δ^7Li (Fig. 7b) confirms this probability, indicating that the Li carried by surface runoff is the main Li source in bauxite-bearing rocks because the positive correlation means that the higher the illite contents are, the higher is the Li absorbed from the water and the higher is the δ^7Li.

Chlorite is a trioctahedral Mg–Fe clay mineral, which is sensitive to chemical weathering and easy to transform into other clay minerals under intense chemical weathering (Zhao et al., 2003). Although chlorite occurs in the Hanjiadian Formation silty shale (Table 2), the chlorite in the Xinmin bauxite deposit was not necessarily completely inherited from the Hanjiadian Formation. Studies have shown that chlorite can be transformed from illite, kaolinite, and pyrophyllite during the diagenetic process, with the participation of Fe- and Mg-enriched fluids under reduced conditions (Cui et al., 2013; Ling et al., 2021). Since pyrophyllite was not found in the Xinmin bauxite deposit (Table 2), chlorite in the Xinmin bauxite deposit should be transformed from illite and/or kaolinite. It can be proven by the negative correlation between illite + kaolinite vs. chlorite in bauxitic rock and aluminous claystone with high clay mineral content (Fig. 8) and by the close symbiotic relationship between chlorite, illite, and kaolinite (Fig. 6a–6c). Due to isotopic fractionation, the secondary chlorite has a lower δ^7Li than that of precursor mineral, resulting in a negative correlation between chlorite and δ^7Li (Fig. 7d). During diagenesis, if there was Li-rich fluid, illite and/or kaolinite could react with it to form Li-chlorite (Ling et al., 2021). However, Li-chlorite was not found in the Xinmin deposit, indicating that the pore water in the diagenetic stage was short of Li, which is also confirmed by no obvious correlation between chlorite and Li contents (Fig. 7c).

Kaolinite occurs in various rocks of the Xinmin deposit (Table 2). Since there is limited kaolinite in the Hanjiadian Formation (Table 2), most kaolinite in the Xinmin bauxite deposit should be from illite hydrolysis in the Hanjiadian Formation under acidic conditions (Cui et al., 2013). The kaolinization in illite (Fig. 6a) and the close symbiosis between kaolinite and illite (Fig. 6c) simultaneously indicate the genetic relationship between them. Unlike illite, kaolinite has a 1:1 layered structure, and its cation-adsorption capacity is weaker than that of illite. Li ions will be preferentially adsorbed in illite when illite coexists with kaolinite. Thus, although a positive correlation exists between kaolinite and Li contents, the correlation is weaker than that of illite (Fig. 7e). Due to isotopic fractionation, secondary kaolinite has lower δ^7Li than

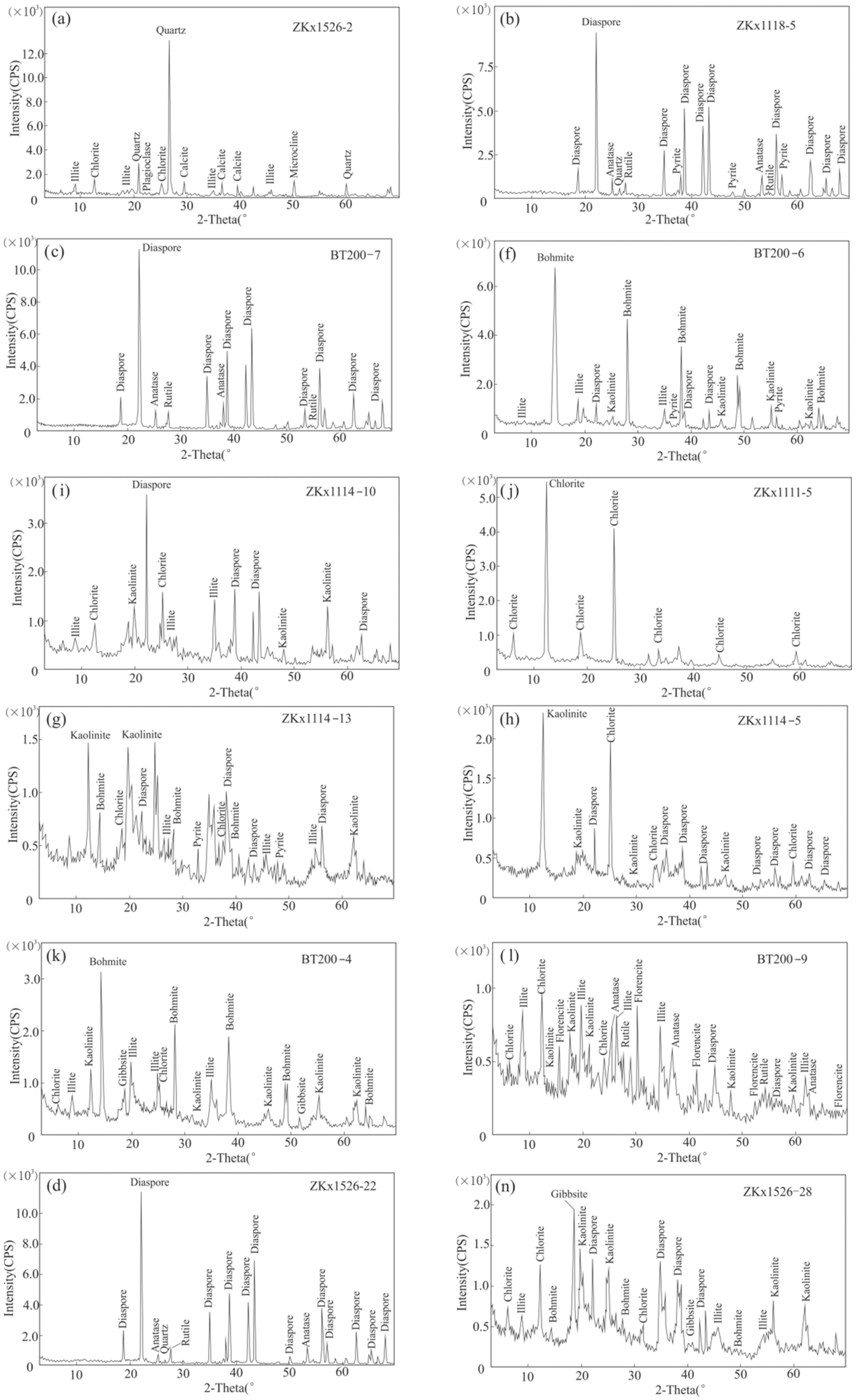

Fig. 3. The XRD patterns for selected samples from the Xinmin bauxite deposit.

precursor mineral (Li and Liu, 2020); however, the Li adsorbed from water with heavy δ^7Li characteristics could increase the δ^7Li. The two offset each other, resulting in no correlation between δ^7Li and kaolinite (Fig. 7f).

In addition, the Li host minerals vary in different lithologies. Illite mainly exists in bauxitic rocks and compact bauxite ores (Table 2), and the Li contents are positively correlated with K_2O (Fig. 9), indicating that illite is a Li host mineral in bauxitic rocks and compact bauxite ores. The clay minerals in aluminous claystone are mainly kaolinite and chlorite (Table 2), and the Li contents do not correlate with K_2O (Fig. 9), indicating that kaolinite is a Li host mineral in aluminous claystone.

Clay mineral compositions are complex in bauxite-bearing rocks.

Table 3
Li contents and δ^7Li of bauxite-bearing rocks from Xinmin bauxite deposit, northern Guizhou, China.

Formation	lithology	δ^7Li(‰)			Li ($\times10^{-6}$)		
		Range	Average	Number of samples	Range	Average	Number of samples
P_2l	Carbonaceous shale	−5.23 ~ 1.56	−0.69	4	27.85 ~ 103.59	64.89	6
P_1d	Aluminous claystone	−2.96 ~ 3.48	0.21	11	201.01 ~ 1384.03	839.15	11
	Bauxitic rock	−0.83 ~ 2.41	1.47	7	727.39 ~ 3521.36	1724.87	7
	Compact bauxite ore	−0.91 ~ 1.81	1.11	9	355.53 ~ 1994.23	803.84	9
	Pelitomorphic bauxite ore	−1.05 ~ 1.75	0.77	3	1.68 ~ 69.68	16.34	11
	Whole strata	**−2.96 ~ 3.48**	**0.83**	**30**	**1.68 ~ 3521.36**	**755.77**	**38**
C_2h	Limestone	−10.33		1	6.8 ~ 21.45	11.99	6
$S_{1\text{-}2}hj$	Silty shale	−0.54 ~ -0.43	−0.47	3	37.99 ~ 62.47	48.53	6

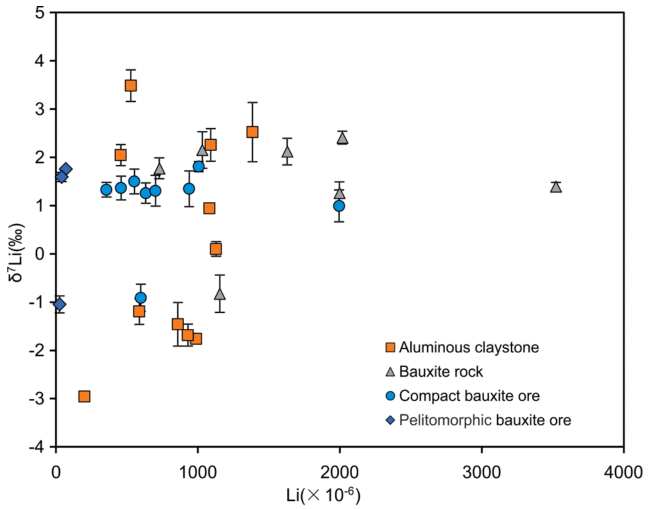

Fig. 4. Variation plots of Li ($\times10^{-6}$) versus δ^7Li (‰) for samples from the Xinmin bauxite deposit.

Some clay minerals cannot be detected using XRD because of their small particles or poor crystallinity, but they might be Li host minerals, such as smectite (Wen et al., 2020; Ling et al., 2020). Smectite has a typical 2:1 layered structure with a high negative charge and large specific surface area, and its ability to adsorb cations is stronger than that of illite and kaolinite. Wen et al. (2020) and Ling et al. (2020) considered that Li in bauxite-bearing rocks mostly occurs in smectite in the form of adsorption. In addition to Mg, smectite contains some Na. In this study, the weak positive correlations between Li vs. MgO and Na_2O, respectively, (Fig. 10) indicate that smectite is the Li host mineral in the Xinmin deposit, but the correlation between Li vs. MgO is weaker than that of Li vs. Na_2O might be affected by Mg from chlorite (Fig. 10).

5.3. *Enrichment mechanism of Li in the Xinmin bauxite deposit*

The Li enrichment mechanism in the Xinmin bauxite deposit is related to the metallogenic process of bauxite. The Xinmin bauxite deposit is a PCS type bauxite deposit (Zhong et al., 2019), and its formation of Xinmin bauxite deposit includes the primary bauxitic material formation stage, the burial and diagenesis stage, and the supergene leaching stage (Gu et al., 2013). To clarify the Li enrichment mechanism, at least two questions must be answered. (1) In what stage did Li

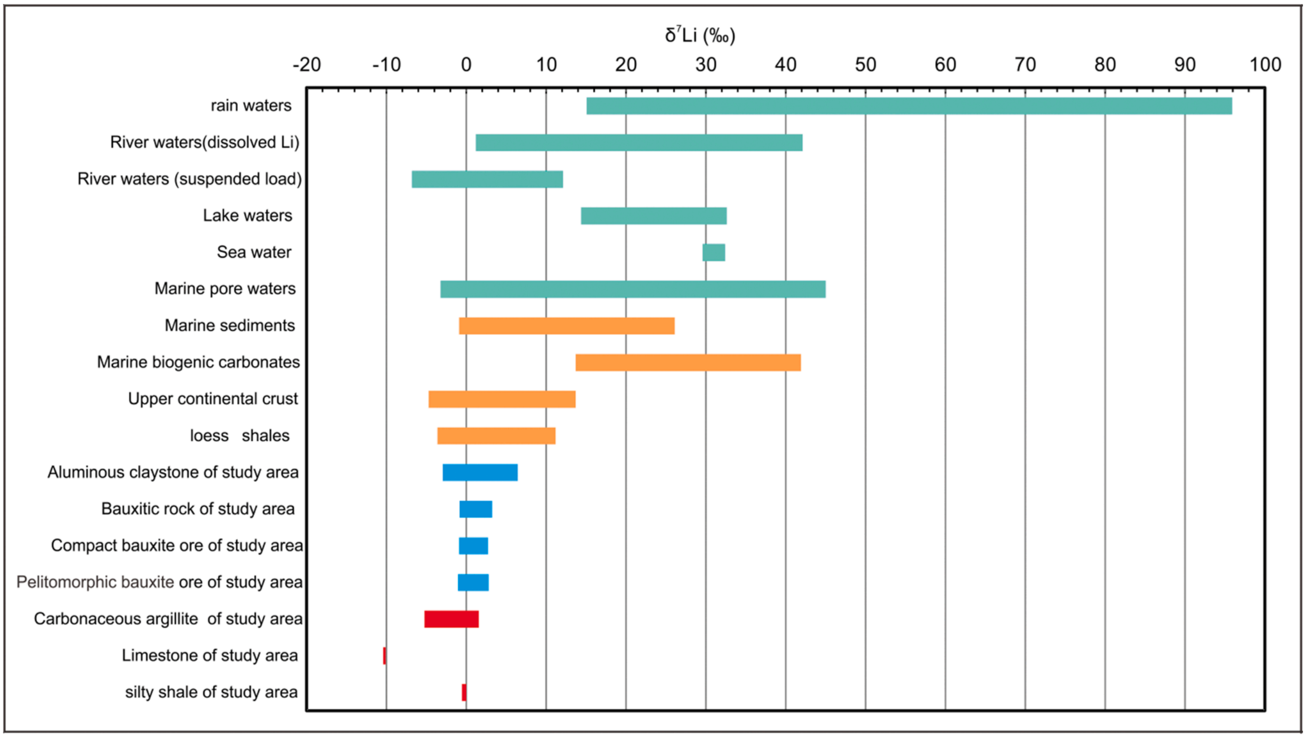

Fig. 5. δ^7Li in different reservoirs on the surface of the Earth and different lithologies of the Xinmin bauxite deposit (Modified after Tomascak, 2004; Tomascak et al., 2008; Tang et al., 2009; Tomascak et al., 2016; Penniston-Dorland et al., 2017).

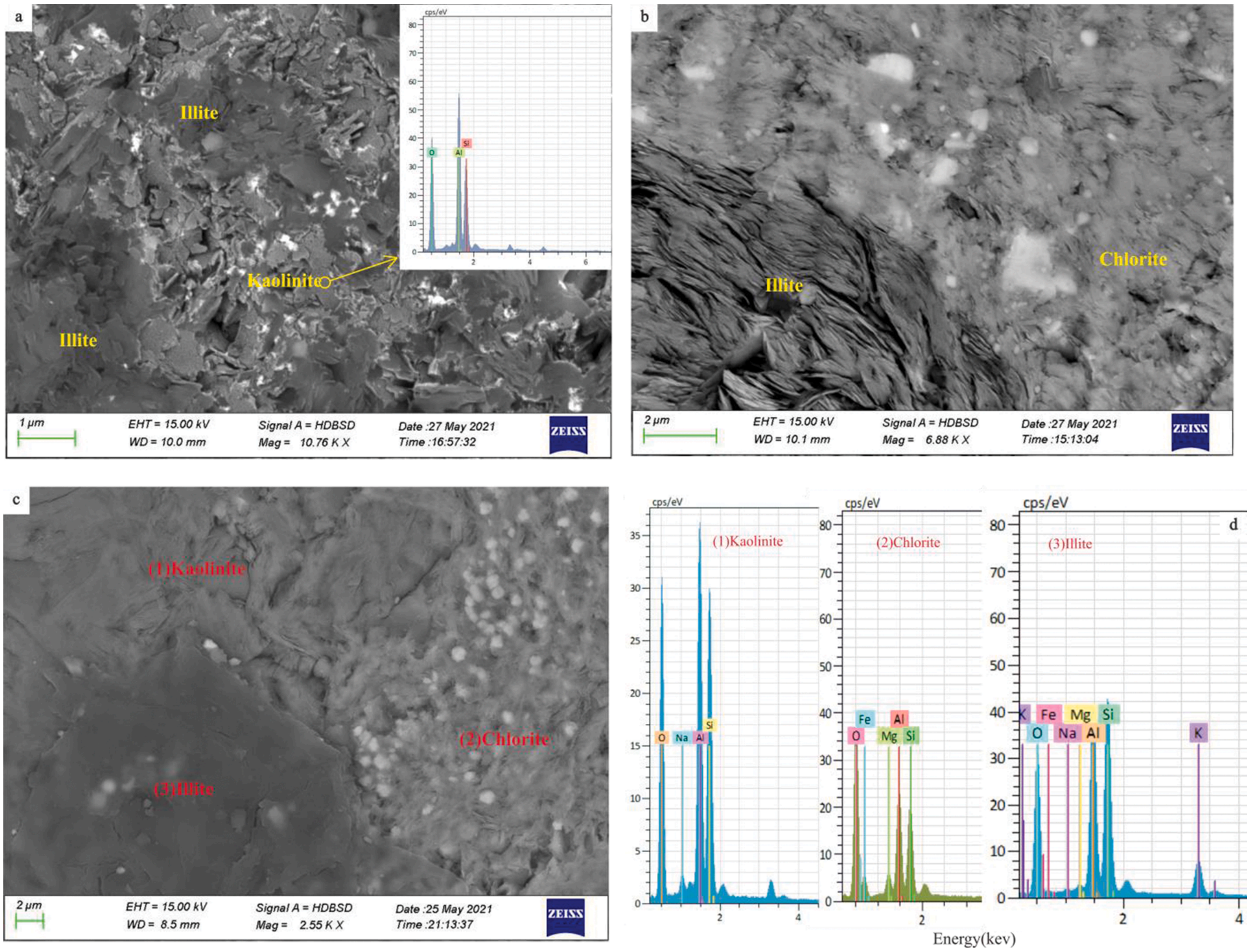

Fig. 6. SEM images of bauxitic rock (ZKx1526-28) in Xinmin bauxite deposit. (a) Kaolinite alteration on illite surface; (b) Illite coexisting with chlorite; (c) Illite, kaolinite and chlorite coexisting; (d) SEM-EDS analysis energy spectrum of part of illite, kaolinite and chlorite.

enrichment occur during bauxite formation? (2) What factors contributed to Li enrichment?

At the supergene leaching stage, the formed bauxite-bearing rocks were lifted to near the surface due to tectonic movement. Under strong surface water leaching, Li in bauxite-bearing rocks could be locally leached. Therefore, it was unlikely to increase Li contents in bauxite at the supergene leaching stage. At the burial and diagenesis stage, the primary bauxitic materials were compacted and consolidated under the pressure of overlying sediments. At that time, the sediments were in a relatively closed environment. If the pore water was Li enriched, it could react with illite and/or kaolinite to form Li-chlorite. However, Li-chlorite was not found in the Xinmin deposit, indicating that the Li was depleted in the pore water during the burial diagenesis stage, indicating that the Li enrichment occurred before the burial and diagenesis stage in the Xinmin bauxite deposit.

From the above mentioned analysis, the Li enrichment of bauxite-bearing rocks should occur at the primary bauxitic material formation stage, where the ore-forming parent rocks had decomposed under intense weathering. The weathering products accumulated in depressions in situ or after short-distance transportation and were subjected to strong laterization to form primary bauxitic materials. Furthermore, all strata in the basin, including the ore-forming parent rocks, were subjected to intense weathering. In the process, Li isotopes fractionated, ^{6}Li was preferentially retained in secondary minerals, and ^{7}Li entered the surface runoff and converged into the restricted basin of primary bauxitic material deposition. However, whether the imported Li can be enriched in the primary bauxitic materials was closely related to the sedimentary basin type and the hydrological and climatic conditions at that time. The Xinmin bauxite deposit formed in the coastal restricted basin (Li et al., 2013), and the sea level considerably affected the groundwater level. If the sea level and groundwater table were low and rainfall was abundant, the leaching was strong, which was conducive to the high-quality bauxitic horizon formation (Yu et al., 2019). However, the imported Li could not be retained in the basin but discharged from the basin under strong leaching. Therefore, Li contents and δ^{7}Li of the primary bauxitic materials were low. However, if the sea level and groundwater table were high, the retention water body had formed in the restricted basin and the leaching weakened. Although it was not conducive to bauxitic horizon formation, the Li carried by surface runoff could retain in the basin. If the climate was dry and hot, the retention water body gradually alkalized through evaporation and some clay minerals could transform into smectite (Wen et al., 2020). Under further evaporation, illite, kaolinite, and smectite gradually adsorbed the Li in water. This mechanism increases the Li contents and δ^{7}Li of the primary bauxitic materials and reveals low Li contents in high-grade bauxite ores. It also indicates that the migration process of Li carried by surface runoff during the primary bauxitic materials formation stage determined the present Li contents and δ^{7}Li of the bauxite-bearing rocks, and the sedimentary environment, hydrology, and climate at that time controlled the process.

The bauxite deposits in northern Guizhou formed in a coastal restricted basin (Cui, 2020). The restricted environment is not only

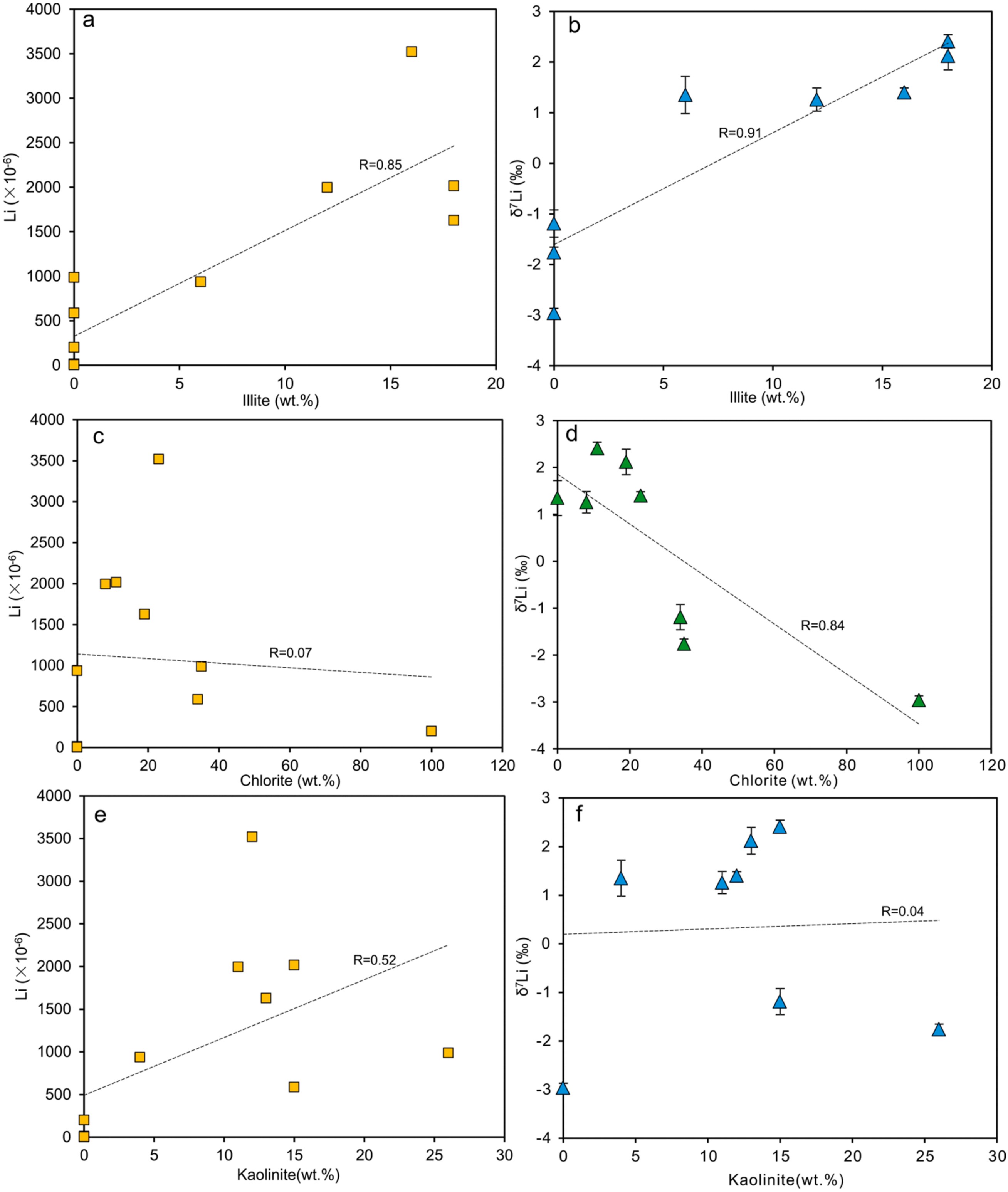

Fig. 7. Correlations beween different clay minerals vs. Li contents and δ^7Li.

conducive to the accumulation of primary bauxitic materials but also becomes an ideal place for collecting Li carried by surface runoff. Therefore, under a favorable sedimentary environment, paleohydrology and paleoclimate conditions become the main factors controlling associated Li enrichment. The study has shown that eustatic change is critical to bauxite mineralization (Yu et al., 2019; Li et al., 2019; Cui, 2020). Its significance is that sea-level rise and fall considerably affect the coastal environment's groundwater level, affecting the strength of leaching. The Carboniferous–Permian bauxite deposits in South China formed in the coastal environment. The high-frequency sea-level change caused by the waxing and waning of Gondwana ice sheets in the Late Paleozoic Ice Age led to frequent changes in the coastal environment's groundwater table, resulting in the constantly changing leaching in the sedimentary environment between strong and weak. When the leaching

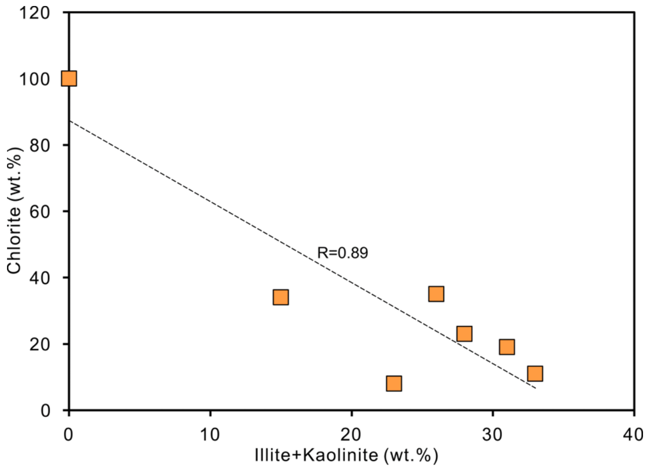

Fig. 8. Correlation beween illite + kaolinite vs. chlorite in bauxitic rock and aluminous claystone.

was strong, high-quality bauxite ores formed, and when the leaching was weak, the bauxitic rocks and aluminous claystone formed (Li et al., 2019; Cui, 2020). According to the bauxite ore types and lithological association, the bauxite deposits in northern Guizhou, China, experienced at least four sea-level changes during their formation (Cui, 2020). During bauxite mineralization in northern Guizhou, China, the hydrological conditions frequently changed due to the sea-level change, changing the strength of leaching in the sedimentary environment, affecting bauxite mineralization and controlling the migration state of Li. The impact of climate on enriching associated Li is whether Li in water can be effectively adsorbed by clay minerals. When the climate is warm and humid, most Li exists in water in a dissolved state. Only when the climate is dry and hot, with water evaporation, can clay minerals gradually adsorb the Li in water. Climate is critical in bauxite formation. Research shows that the alternating climatic conditions of warm–humid and hot–dry are conducive to bauxite formation (Price et al., 1997; Retallack, 2008; Yu et al., 2019). During the Carboniferous–Permian, the South China craton was located in the east of the Paleo–Tethys Ocean and within 30° of the equator with a tropical and subtropical climate (Rixiang et al., 1998; Huang et al., 2001; Yang et al., 2004). The alternation of rainy and dry seasons is conducive to Late Paleozoic bauxite formation in China. Evidence for Permian wildfires, based on discovering combustion-derived polycyclic aromatic hydrocarbons within the Early Permian Dazhuyuan Formation of NGB, imply that the paleoclimate was generally wet with dry intervals in northern Guizhou, China (Yu et al., 2013). In summary, in the Early Permian, favorable or unfavorable conditions occurred for Li enrichment in northern Guizhou, China, in hydrological and climatic conditions. Only when favorable conditions were coupled, was it conducive to Li enrichment.

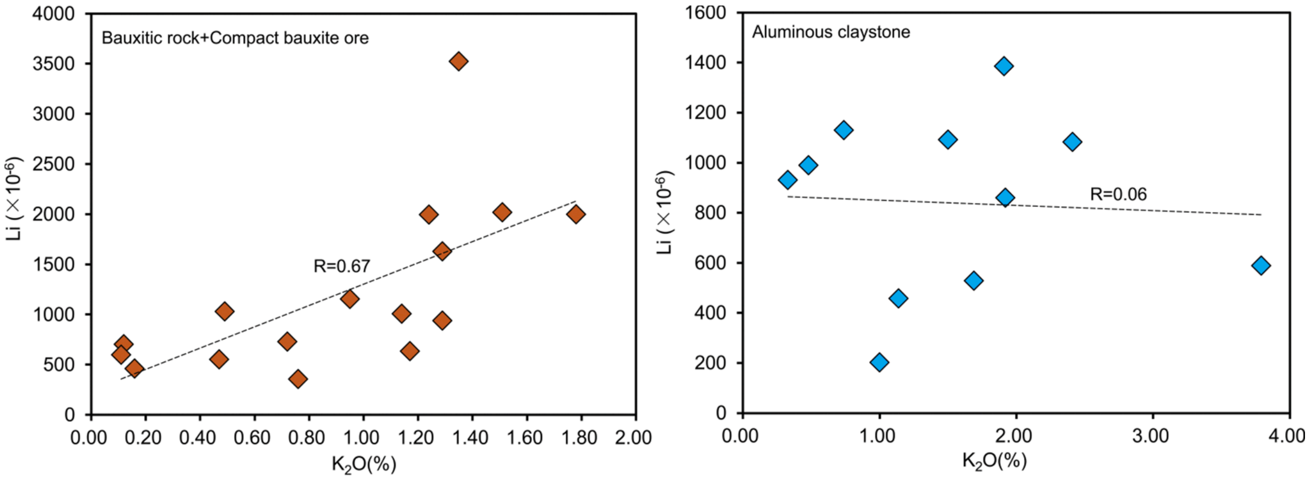

Fig. 9. Correlations beween K_2O vs. Li contents in different lithologies from the Xinmin bauxite deposite.

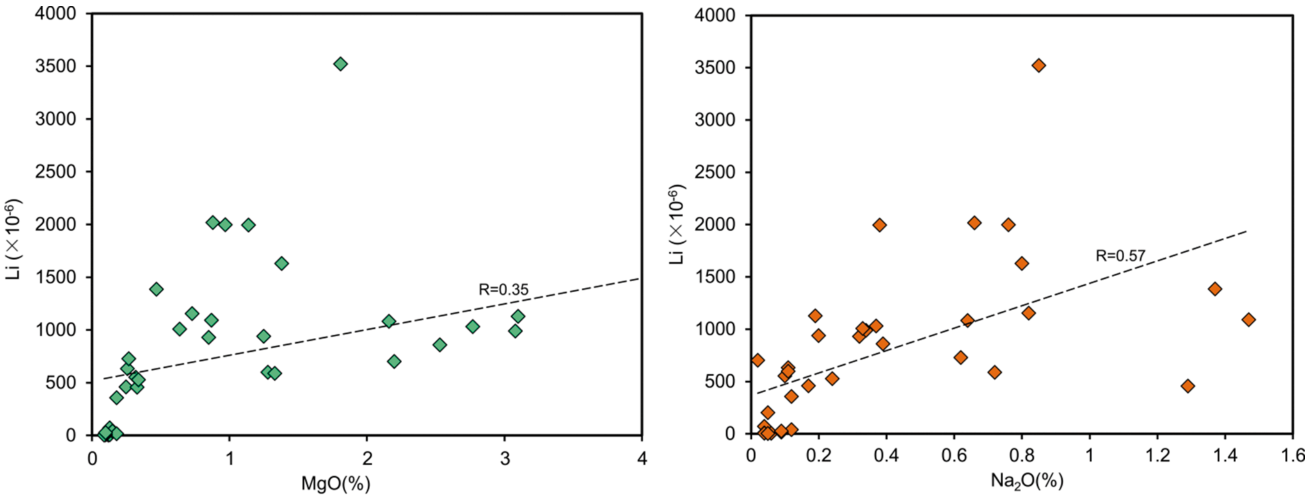

Fig. 10. Correlations beween Li contents vs.MgO and Na_2O in the Xinmin bauxite deposite, respectively.

According to the above, a positive correlation should occur between the δ^7Li and Li contents in the Xinmin bauxite deposit, but no obvious correlation exists between them (Fig. 4). This relationship can be explained by the correlations between δ^7Li and different clay minerals. At the primary bauxitic material formation stage, little chlorite occurred in clay minerals. The clay minerals adsorbing Li mainly comprised illite and kaolinite. Illite was mainly inherited from the ore-forming parent rocks and had a strong adsorption capacity for Li carried by retained

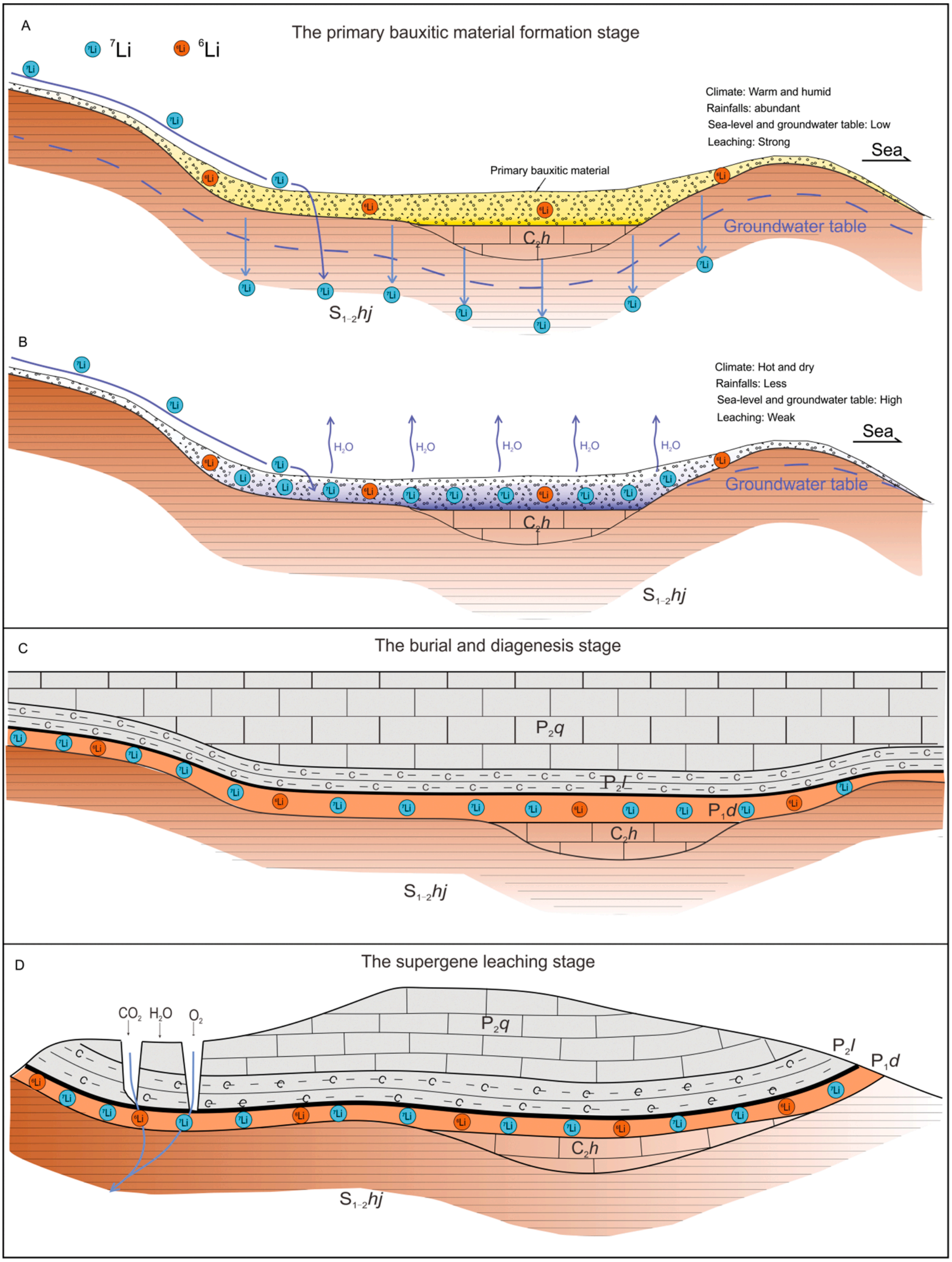

Fig. 11. Enrichment model of associated Li in the Xinmin bauxite deposit, Northern Guizhou Province, China. (A) The climate was warm and humid, the sea level and groundwater table were low, the rainfall was abundant, and the leaching was strong, the Li flowing into the basin was leached out. (B) The climate was dry and hot, the sea level and groundwater table were high, the rainfall was less, the retained water body formed in the basin, and the leaching was weak, the Li flowing into the basin was adsorbed by illite, kaolinite, and smectite. (C) The bauxite deposit initially formed, illite and/or kaolinite in the lower part of the ore-bearing rocks reacted with Li-poor fluid to form chlorite and the composition of clay minerals in the lower part of the ore-bearing rocks changed. (D) The ore-bearing rocks lifted to the surface, under the leaching of strong acid fluid, the distribution state of Li changes locally.

water, resulting in illite vs. Li contents and δ^7Li positively correlating, respectively (Fig. 7a, 7b). Chlorite was transformed from illite and/or kaolinite at the burial and diagenetic stage, but the Li adsorption and enrichment mostly occurred at the primary bauxitic material formation stage. Therefore, no obvious correlation exists between chlorite and Li contents (Fig. 7c); however, the secondary chlorite has a lower δ^7Li (such as ZKx1111-5) than precursor minerals, leading to a negative relationship between δ^7Li and chlorite (Fig. 7d). Kaolinite in the primary bauxitic materials was mainly transformed from the hydrolysis of illite inherited from the Hanjiadian Formation. Kaolinite is positively correlated with Li contents because of its adsorption to Li carried by retained water (Fig. 7e). Secondary kaolinite has low δ^7Li (Li and Liu, 2020), but no correlation exists between δ^7Li and kaolinite (Fig. 7f) due to its adsorption to Li carried by retained water. In summary, the absence of correlations between δ^7Li and Li contents in the Xinmin bauxite deposit is a comprehensive reflection of the relationship between δ^7Li and illite, kaolinite, and chlorite, respectively.

Based on the above discussion, we propose the following model for Li enrichment in the Xinmin bauxite deposit.

In the first stage, the Hanjiadian Formation's silty shale and the Huanglong Formation's limestone decomposed under intense weathering. The weathering products were accumulated in depressions in situ or after short-distance transportation. With surface water, organisms, CO_2, and O_2 participation, the weathering products were subjected to strong laterization to form primary bauxitic materials accompanied by the leaching of Si and numerous alkaline elements (including Li) (Bárdossy, 1982; Bárdossy and Aleva, 1990). Simultaneously, all strata in the basin, including the ore-forming parent rocks, suffered from intense weathering. In this process, ^{7}Li preferentially entered the surface runoff due to Li isotope fractionation and converged into the restricted basin. At that time, if the leaching was strong, the imported Li could not retain in the basin but discharged from the basin under strong leaching (Fig. 11A). However, If the leaching weakened, Li carried by water could retain in the basin and be adsorbed by illite, kaolinite, and smectite with water evaporation under hot and dry climates to increase the Li contents and δ^7Li of the primary bauxitic materials (Fig. 11B).

In the second stage, the sedimentary basin was gradually swamped with organism participation. A set of carbonaceous fine debris sediments began to accumulate on the surface of the primary bauxitic materials. A large-scale transgression completely submerged the basin, and sediments gradually covered the surface of original bauxite horizons, and the overlying Liangshan and Qixia Formations formed (Fig. 11C). Under the pressure of overlying sediments, the bauxite deposit initially formed. Simultaneously, illite and/or kaolinite reacted with alkaline and Li-poor fluids to form chlorite in the lower part of bauxite-bearing rocks.

In the third stage, the bauxite deposit was lifted to near the surface due to tectonic movement. Consequently, pyrite in the overlying Liangshan Formation was oxidized, generating SO_4^{2-} and mixed with surface water and CO_2 to form a strong acid fluid, comprising sulfuric, carbonic, and humic acids. The strong acid fluid decomposed clay minerals in the ore bed and improved the quality of bauxite ores. When it flowed through some ore beds with good permeability, most clay minerals would decompose. Li also leached out, and high-grade bauxite ores with low Li contents, comprising diaspore and heavy minerals, formed (Fig. 11D). However, surface water easily diluted the high acid fluids and rock joints and fissures strictly controlled the flowing paths. Therefore, the leaching process could only have a local impact on Li and δ^7Li distribution in bauxite-bearing rocks.

Due to the similar sedimentary environments of paleohydrological and paleoclimatic conditions during the PCS type bauxite deposit formation, the model is also suitable for the PCS type bauxite deposits in other parts of China. It is the reason why a PCS type bauxite deposit is typically rich in associated Li resources.

6. Conclusions

1) At least two Li sources occur in the Xinmin bauxite deposit, namely, parent rocks and surface runoff. Surface runoff with heavy δ^7Li characteristics should be the major source.

2) The Li host minerals in the Xinmin deposit are mainly illite and kaolinite and probably smectite. Li in bauxitic rocks and compact bauxite ores is mainly hosted in illite, whereas Li in aluminous claystone is mainly hosted in kaolinite.

3) Li enrichment occurred at the primary bauxitic material formation stage. Under hot and dry climates, the coastal restricted basin with retention water after small-scale transgression is conducive to Li enrichment.

Declaration of Competing Interest

The authors declare that they have no known competing financial interests or personal relationships that could have appeared to influence the work reported in this paper.

Acknowledgments

The two anonymous reviewers are thanked for their constructive suggestions, which have greatly improved the quality of this paper. This study was supported by the special topic of deep earth resources exploration and exploitation in national key R&D plan (No. 2017YFC0602701), the Geological chronicle of China mineral resources project of China Geological Survey (No. DD20160346, DD20190379), the National Key R&D Program of China (2021YFC2900092), and the Project of Guizhou Province talent base (No. RCJD2018-21).

References

Bárdossy, G., 1982. Karst bauxites, bauxite deposits on carbonate rocks. Developments in economic geology 14. Elsevier, Amsterdam, pp. 1–441.

Bárdossy, G., Aleva, G.J.J., 1990. Lateritic Bauxites. Elsevier Scientific Publication, Amsterdam, pp. 1–624.

Lui-Heung, C., Edmond, J.M., 1988. Variation of lithium isotope composition in the marine environment: A preliminary report. Geochim. Cosmochim. Acta. 52 (6), 1711–1717.

Cui, T., Jiao, Y.Q., Du, Y.S., Wang, X.M., Lei, Z.Y., Weng, S.F., 2013. Mineralogical and geochemical characteristic of bauxite in Northern Guizhou. The Chinese Journal of Nonferrous Metals. 23 (10), 2905–2920 in Chinese with English abstract.

Cui, T., 2020. Key control factor in ore-forming process of bauxite in northern Guizhou—Sea level changes. The Chinese Journal of Nonferrous Metals. 30 (6), 1466–1479 in Chinese with English abstract.

Franzini, M., Leoni, L., Saitta, M., 1972. A simple method to evaluate the matrix effects in X-ray fluorescence analysis. X-Ray Spectrom. 1 (4), 151–154.

Godfrey, L.V., Chan, L.-H., Alonso, R.N., Lowenstein, T.K., McDonough, W.F., Houston, J., Li, J., Bobst, A., Jordan, T.E., 2013. The role of climate in the accumulation of lithium-rich brine in the Central Andes. Applied Geochemistry. 38, 92–102.

Gu, J., Huang, Z.L., Fan, H.P., Ye, L., Jin, Z.G., 2013. Provenance of lateritic bauxite deposits in the Wuchuan-Zheng'an-Daozhen area, Northern Guizhou Province, China: LA-ICP-MS and SIMS U-Pb dating of detrital zircons. Journal of Asian Earth Sciences. 70–71 (2013), 265–282.

Hathorne, E., James, R., 2006. Temporal record of lithium in seawater: A tracer for silicate weathering. Earth Planet. Sci. Lett. 246 (3-4), 393–406.

Henchiri, S., Clergue, C., Dellinger, M., Gaillardet, J., Louvat, P., Bouchez, J., 2014. The influence of hydrothermal activity on the Li isotopic signature of rivers draining volcanic areas. Procedia Earth and Planetary Science. 10, 223–230.

He, M.Y., Dong, J.B., Jin, Z.D., Liu, C.Y., Xiao, J., Zhang, F., Sun, H., Zhao, Z.Q., Gou, L. F., Liu, W.G., Luo, C.G., Song, Y.G., Ma, L., Deng, L.i., 2021. Pedogenic processes in loess-paleosol sediments: Clues from Li isotopes of leachate in Luochuan loess. Geochim. Cosmochim. Acta. 299 (2021), 151–162.

Hindshaw, R.S., Tosca, R., Goût, T.L., Farnan, I., Tosca, N.J., Tipper, E.T., 2019. Experimental constraints on Li isotope fractionation during clay formation. Geochim. Cosmochim. Acta. 250, 219–237.

Huang, B., Otofuji, Y.-I., Zhu, R., Shi, R., Wang, Y., 2001. Paleomagnetism of Carboniferous sediments in the Hexi corridor: its origin and tectonic implications. Earth Planet. Sci. Lett. 194 (1-2), 135–149.

Huh, Y., Chan, L.H., Chadwick, O., 2002. Lithium isotopes as a probe of weathering processes: Hawaiian soil climosequence. Geochim. Cosmochim. Acta. 66 (15A), A346.

Huh, Y., Chan, L.-H., Chadwick, O.A., 2004. Behavior of lithium and its isotopes during weathering of Hawaiian basalt. Geochemistry Geophysics, Geosystems. 5 (9), n/a–n/a.

Jin, Z.G., Liu, L., Huang, Z.L., Liu, C.S., Zheng, M.H., Gu, J., Zou, L., Wang, L., 2019. Occurrence state, enrichment mechanism and resource potential of rare earth, rare metal and rare-scattered elements in ore-bearing rocks in the Wuchuan-Zheng'an-Daozhen bauxite deposit. Guizhou Province. Acta Geologica Sinica. 93 (11), 2847–2861 in Chinese with English abstract.

Ji, H., Chang, C., Beckford, H.O., Song, C., Blake, R.E., 2021. New perspectives on lateritic weathering process over karst area-Geochemistry and Si-Li isotopic evidence. Catena 198, 105022. https://doi.org/10.1016/j.catena.2020.105022.

Karayigit, A.I., Bulut, Y., Karayigit, G., Querol, X., Alastuey, A., Vassilev, S., Vassileva, C., 2006. Mass balance of major and trace elements in a coal-fired power plant. Energ. Source. Part A 28 (14), 1311–1320.

Kısakürek, B., Widdowson, M., James, R.H., 2004. Behaviour of Li isotopes during continental weathering: The Bidar laterite profile. India. Chemical Geology. 212 (1-2), 27–44.

Kısakűrek, B., James, R.H., Harris, N.B.W., 2005. Li and δ^7Li in Himalayan rivers: Proxies for silicate weathering. Earth Planet. Sci. Lett. 237 (3-4), 387–401.

Liu, X.-M., Rudnick, R.L., 2011. Constraints on continental crustal mass loss via chemical weathering using lithiumand its isotopes. Proceedings of the National Academy of Sciences of the United States of America. 108 (52), 20873–20880.

Liu, X.-M., Rudnick, R.L., McDonough, W.F., Cummings, M.L., 2013. Influence of chemical weathering on the composition of the continental crust: Insights from Li and Nd isotopes in bauxite profiles developed on Columbia River Basalts. Geochim. Cosmochim. Acta. 115, 73–91.

Li, Z.H., Din, J., Xu, J.S., Liao, C.G., Yin, F.G., Lu, T., Cheng, L., Li, J.M., 2013. Discovery of the REE minerals in the Wulong-Nanchuan bauxite deposits, Chongqing, China: Insights on conditions of formation and processes. Journal of Geochemical Exploration. 133 (2013), 88–102.

Li, P., Yu, W., Du, Y., Lai, X., Weng, S., Pang, D., Xiong, G., Lei, Z., Zhao, S., Yang, S., 2020. Influence of geomorphology and leaching on the formation of Permianbauxite in northern Guizhou Province, South China. Journal of Geochemical Exploration. 210, 106446. https://doi.org/10.1016/j.gexplo.2019.106446.

Li, W., Liu, X.-M., 2020. Experimental investigation of lithium isotope fractionation during kaolinite adsorption: Implications for chemical weathering. Geochim. Cosmochim. Acta. 284, 156–172.

Ling, K.-Y., Zhu, X.-Q., Tang, H.-S., Du, S.-J., Gu, J., 2018. Geology and geochemistry of the Xiaoshanba bauxite deposit, Central Guizhou Province, SW China: Implications for the behavior of trace and rare earth elements. J Geochem. Explor. 190, 170–186.

Ling, K.-Y., Tang, H.-S., Zhang, Z.-W., Wen, H.-J., 2020. Host minerals of Li–Ga–V–rare earth elements in Carboniferous karstic bauxites in southwest China. Ore Geology Reviews 119, 103325. https://doi.org/10.1016/j.oregeorev.2020.103325.

Ling, K.Y., Wen, H.J., Zhang, Q.Z., Luo, C.G., Gu, H.L., Du, S.J., Yu, W.X., 2021. Super-enrichment of lithium and niobium in the upper Permian Heshan Formation in Pingguo, Guangxi. China. Science China Earth Sciences. 64 (5), 753–772 in Chinese with English abstract.

Long, K.S., Fu, Y., Chen, R., Ye, Y.M., Yan, S., Chen, M.Z., 2019. The REE enrichment mechanism of bauxite deposits in the Northern Guizhou: A case study of the Xinmin bauxite deposit. Acta Mineralogica Sinica 39 (4), 443–454 in Chinese with English abstract.

Long, Z., Fu, Y., He, W., Tang, B., Long, K.S., Liu, Y., Wang, T.S., 2021. Geochemical characteristics and enrichment mechanism of Li in Xinmin bauxite deposit. Guizhou. Mineral Deposits. 40 (4), 873–890 in Chinese with English abstract.

Misra, S., Froelich, F., 2012. Lithium isotope history of Cenozoic seawater: Changes in silicate weathering and reverse weathering. Science 335 (6070), 818–823.

Penniston-Dorland, S., Liu, X.M., Rudnick, R.L., 2017. Lithium Isotope Geochemistry. Reviews in Mineralogy & Geochemistry. 82 (2017), 165–217.

Pistiner, J.S., Henderson, G.M., 2003. Lithium isotope fractionation during continental weathering processes. Earth Planet. Sci. Lett. 214 (1-2), 327–339.

Potts, P.J., Thompson, M., Kane, J.S., Petrov, L.L., 2000. GEOPT7–an international proficiency test for analytical geochemistry laboratories. In: Report on Round 7, 35.

Potts, P.J., Thompson, M., Webb, P.C., Watson, J.S., 2001. GEOPT9–an international proficiency test for analytical geochemistry laboratories. In: Report on Round 9, 36.

Pogge von Strandmann, P.A.E., Burton, K.W., James, R.H., van Calsteren, P., Gíslason, S.R., Mokadem, F., 2006. Riverine behaviour of uraniumand lithium isotopes in an actively glaciated basaltic terrain. Earth Planet. Sci. Lett. 251 (1-2), 134–147.

Price, G.D., Valdes, P.J., Sellwood, B.W., 1997. Prediction of modern bauxite occurrence: implications for climate reconstruction. Palaeogeogr. Palaeoclimatol. Palaeoecol. 131 (1-2), 1–13.

Qi, L., Hu, J., Gregoire, D.C., 2000. Determination of trace elements in granites by inductively coupled plasma mass spectrometry. Talanta 51, 507–513.

Retallack, G.J., 2008. Cool-climate or warm-spike lateritic bauxites at high latitudes? Journal of Geology. 116 (6), 558–570.

Rudnick, R.L., Tomascak, P.B., Njo, H.B., Gardner, L.R., 2004. Extreme lithium isotopic fractionation during continental weathering revealed in saprolites from South Carolina. Chemical Geology. 212 (1-2), 45–57.

Ryu, J.-S., Vigier, N., Lee, S.-W., Lee, K.-S., Chadwick, O.A., 2014. Variation of lithium isotope geochemistry during basalt weathering and secondary mineral transformations in Hawaii. Geochim. Cosmochim. Acta. 145, 103–115.

Sauzéat, L., Rudnick, R.L., Chauvel, C., Garçon, M., Tang, M., 2015. New perspectives on the Li isotopic composition of the upper continental crust and its weathering signature. Earth Planet. Sci. Lett. 428, 181–192.

Steinhoefel, G., Brantley, S.L., Fantle, M.S., 2021. Lithium isotopic fractionation during weathering and erosion of shale. Geochim. Cosmochim. Acta. 295 (2021), 155–177.

Tang, Y.J., Zhang, H.F., Ying, J.F., 2009. Discussion on Fractionation Mechanism of Lithium Isotopes. Earth Science-Journal of China University of Geosciences. 34 (1), 43–55 in Chinese with English abstract.

Teng, F.-Z., Li, W.-Y., Rudnick, R.L., Gardner, L.R., 2010. Contrasting lithium and magnesium isotope fractionation during continental weathering. Earth Planet. Sci. Lett. 300 (1-2), 63–71.

Thompson, M., Potts, P.J., Kane, J.S., Wilson, S., 1999. GEOPT5–an international proficiency test for analytical geochemistry laboratories. In: Report on Round 5, 23.

Tomascak, P.B., Hemming, N.G., Hemming, S.R., 2003. The lithium isotopic composition of waters of the Mono Basin. California. Geochim. Cosmochim. Acta. 67 (4), 601–611.

Tomascak, P.B., 2004. Developments in the understanding and applicationof lithium isotopes in the earth and planetary sciences. Reviews in Mineralogy and Geochemistry. 55 (1), 153–195.

Tomascak, P.B., Langmuir, C.H., le Roux, P.J., Shirey, S.B., 2008. Lithium isotopes in global mid-ocean ridge basalts. Geochim. Cosmochim. Acta. 72 (6), 1626–1637.

Tomascak, P.B., Magna, T., Dohmen, D., 2016. Advances in Lithium Isotope Geochemistry. Switzerland: Springer International Publishing, https://doi.org/10.1007/978-3-319-01430-2.

Tsai, P.H., You, C.F., Huang, K.F., Chung, C.H., Sun, Y.B., 2014. Lithium distribution and isotopic fractionation during chemical weathering and soil formation in a loess profile. Journal of Asian Earth Sciences. 87 (2014), 1–10.

Vigier, N., Decarreau, A., Millot, R., Carignan, J., Petit, S., France-Lanord, C., 2008. Quantifying Li isotope fractionation during smectite formation and implications for the Li cycle. Geochim. Cosmochim. Acta. 72 (3), 780–792.

Vigier, N., Gislason, S.R., Burton, K.W., Millot, R., Mokadem, F., 2009. The relationship between riverine lithium isotope composition and silicate weathering rates in Iceland. Earth Planet. Sci. Lett. 287 (3-4), 434–441.

Wang, D., Li, P., Qu, W., Yin, L., Zhao, Z., Lei, Z., Wen, S., 2013. Discovery and preliminary study of the high tungsten and lithium contents in the Dazhuyuan bauxite deposit, Guizhou. China. Science China: Earth Sciences. 56 (1), 145–152.

Wen, H.J., Luo, C.G., Du, S.J., Yu, W.X., Gu, H.N., Ling, K.Y., Cui, Y., Li, Y., Yang, J.H., 2020. Carbonate-hosted clay-type lithium deposit and its prospecting significance. Science china press. 65 (1), 53–59 in Chinese with English abstract.

Williams, L.B., Hervig, R.L., 2005. Lithium and boron isotopesin illite-smectite: The importance of crystal size. Geochim. Cosmochim. Acta. 69 (24), 5705–5716.

Wimpenny, J., James, R.H., Burton, K.W., Gannoun, A., Mokadem, F., Gíslason, S.R., 2010. Glacial effects on weathering processes: New insights from the elemental and lithium isotopic composition of West Greenland rivers. Earth Planet. Sci. Lett. 290 (3-4), 427–437.

Wimpenny, J., Colla, C.A., Yu, P., Yin, Q.-Z., Rustad, J.R., Casey, W.H., 2015. Lithium isotope fractionation during uptake by gibbsite. Geochim. Cosmochim. Acta. 168, 133–150.

Witherow, R.A., Lyons, W.B., Henderson, G.M., 2010. Lithium isotopic composition of the McMurdo Dry Valleys aquatic systems. Chemical Geology. 275 (3-4), 139–147.

Yang, Z., Sun, Z., Yang, T., Pei, J., 2004. A long connection (750–380 Ma) between South China and Australia: paleomagnetic constraints. Earth Planet. Sci. Lett. 220 (3-4), 423–434.

Yan, S., Huang, K.J., Fu, Y., Bao, Z.A., Ma, L., Long, K.S., Ye, Y.M., Chen, R., Chen, M.Z., 2020. Development of separating and purifying methods for Lithium isotope analysis of bauxite. Rock and Mineral Analysis. 39 (1), 41–52 in Chinese with English abstract.

Yu, W.C., Du, Y.S., Wang, X.M., Huang, X., Cui, T., Yu, J.X., Qin, Y.J., 2013. Combustion-derived polycyclic aromatic hydrocarbons in bauxite deposit of Wuchuan-Zheng'an-Daozhen Area, northern Guizhou Province and significance of paleoclimate. Geol. Sci. Technol. Inform. 32 (1), 57–61. In Chinese with English abstract.

Yu, W., Algeo, T.J., Yan, J., Yang, J., Du, Y., Huang, X., Weng, S., 2019. Climatic and hydrologic controls on upper Paleozoic bauxite deposits in South China. Earth-Science Reviews. 189, 159–176.

Rixiang, Z., Zhenyu, Y., Hanning, W.u., Xinghua, M.a., Baochun, H., Zifang, M., Dajun, F., 1998. Paleomagnetic constraints on the tectonic history of the major blocks of China during the Phanerozoic. Sci. China(Series D). 41 (S2), 1–19.

Zhao, L., Ji, J.F., Chen, J., Liu, L.W., Chen, Y., Lu, H.Y., 2003. Chemical weathering of chlorite in Chinese loess-paleosol Sequences in the last 130 ka and climate change. Acta Mineralogica Sinica. 23 (2), 163–168 in Chinese with English abstract.

Zhong, H.R., Sun, Y., Yang, Y.Q., Wang, D.H., Huang, F., Zhao, Z., 2019. Bauxite (aluminum)-type lithium resources and analysis of its development and utilization potential. Mineral Deposits. 38 (4), 898–916 in Chinese with English abstract.